NAVAL POSTGRADUATE SCHOOL

MONTEREY, CALIFORNIA

THESIS

WING-EMBEDDED, CROSS-FLOW-FAN, VERTICAL TAKEOFF AND LANDING AIR VEHICLE

by

Jeremiah J. Fulton

June 2016

Thesis Advisor: Garth V. Hobson
Co-Advisor: Anthony J. Gannon

Approved for public release; distribution is unlimited

THIS PAGE INTENTIONALLY LEFT BLANK

REPORT DOCUMENTATION PAGE			Form Approved OMB No. 0704-0188

1. AGENCY USE ONLY *(Leave blank)*	2. REPORT DATE June 2016	3. REPORT TYPE AND DATES COVERED Master's thesis

4. TITLE AND SUBTITLE
WING-EMBEDDED, CROSS-FLOW-FAN, VERTICAL TAKEOFF AND LANDING AIR VEHICLE

5. FUNDING NUMBERS
TDSI/11–007/1A – NPS

6. AUTHOR(S) Jeremiah J. Fulton

7. PERFORMING ORGANIZATION NAME(S) AND ADDRESS(ES)
Naval Postgraduate School
Monterey, CA 93943-5000

8. PERFORMING ORGANIZATION REPORT NUMBER

9. SPONSORING /MONITORING AGENCY NAME(S) AND ADDRESS(ES)
TDSI-National University of Singapore
21 Lower Kent Ridge Road
Singapore, 119077

10. SPONSORING / MONITORING AGENCY REPORT NUMBER

11. SUPPLEMENTARY NOTES The views expressed in this thesis are those of the author and do not reflect the official policy or position of the Department of Defense or the U.S. Government. IRB Protocol number ____N/A____.

12a. DISTRIBUTION / AVAILABILITY STATEMENT
Approved for public release; distribution is unlimited

12b. DISTRIBUTION CODE

13. ABSTRACT (maximum 200 words)

This research demonstrated that a vertical takeoff and landing aircraft capable of transitioning to conventional flight using cross-flow fans is possible. In particular, the design and manufacture of a wing-embedded cross-flow fan airfoil, and its implementation into an aircraft, was conducted. The design was developed based on the Gottingen 570 airfoil and generated lift coefficients of four—greater than the sum of the parts—due to the fundamental coupling between the wing and cross-flow fan. The wing was characterized with Ansys' CFX solver over tip-speed ratios of zero (hover) to infinity (glide), and predicted a hover angle of 36º with 56% of the lift coming from the airfoil. This meant that a full 90º rotation was not required to go from hover to forward flight; additionally, even while hovering, more than half of the lift was generated by the airfoil.

The airfoil was manufactured from pre-impregnated carbon fiber using a mold produced by 3D printing. Printer filament selection was based on glass transition temperature and printability. ABS filament was chosen due to its high temperature resistance and relative ease of 3D printing.

The aircraft was configured with all the wing assemblies facing the same direction to favor faster forward flight. This differed from previous designs, which used symmetry to increase stability. Controlled untethered flight was successful.

14. SUBJECT TERMS
heavy lifting aircraft, air vehicle, propulsive wing, wing embedded, cross-flow fan (CFF), vertical takeoff and landing (VTOL), horizontal takeoff and landing, 3D print mold, additive material manufacture, prepreg carbon fiber layup, pre-impregnated, controller stabilized

15. NUMBER OF PAGES
109

16. PRICE CODE

17. SECURITY CLASSIFICATION OF REPORT	18. SECURITY CLASSIFICATION OF THIS PAGE	19. SECURITY CLASSIFICATION OF ABSTRACT	20. LIMITATION OF ABSTRACT
Unclassified	Unclassified	Unclassified	UU

NSN 7540-01-280-5500

Standard Form 298 (Rev. 2-89)
Prescribed by ANSI Std. 239-18

THIS PAGE INTENTIONALLY LEFT BLANK

Approved for public release; distribution is unlimited

WING-EMBEDDED, CROSS-FLOW-FAN, VERTICAL TAKEOFF AND LANDING AIR VEHICLE

Jeremiah J. Fulton
Ensign, United States Navy
B.S., United States Naval Academy, 2015

Submitted in partial fulfillment of the
requirements for the degree of

MASTER OF SCIENCE IN MECHANICAL ENGINEERING

from the

NAVAL POSTGRADUATE SCHOOL
June 2016

Approved by: Garth V. Hobson
Thesis Advisor

Anthony J. Gannon
Co-Advisor

Garth V. Hobson
Chair, Department of Mechanical and Aerospace Engineering

THIS PAGE INTENTIONALLY LEFT BLANK

ABSTRACT

This research demonstrated that a vertical takeoff and landing aircraft capable of transitioning to conventional flight using cross-flow fans is possible. In particular, the design and manufacture of a wing-embedded cross-flow fan airfoil, and its implementation into an aircraft, was conducted. The design was developed based on the Gottingen 570 airfoil and generated lift coefficients of four—greater than the sum of the parts—due to the fundamental coupling between the wing and cross-flow fan. The wing was characterized with Ansys' CFX solver over tip-speed ratios of zero (hover) to infinity (glide), and predicted a hover angle of 36º with 56% of the lift coming from the airfoil. This meant that a full 90º rotation was not required to go from hover to forward flight; additionally, even while hovering, more than half of the lift was generated by the airfoil.

The airfoil was manufactured from pre-impregnated carbon fiber using a mold produced by 3D printing. Printer filament selection was based on glass transition temperature and printability. ABS filament was chosen due to its high temperature resistance and relative ease of 3D printing.

The aircraft was configured with all the wing assemblies facing the same direction to favor faster forward flight. This differed from previous designs, which used symmetry to increase stability. Controlled untethered flight was successful.

THIS PAGE INTENTIONALLY LEFT BLANK

TABLE OF CONTENTS

LIST OF FIGURES

THIS PAGE INTENTIONALLY LEFT BLANK

LIST OF TABLES

THIS PAGE INTENTIONALLY LEFT BLANK

LIST OF ACRONYMS AND ABBREVIATIONS

A	Wing Planform Area [m^2]
AOA	Angle of Attack [º]
ABS	Acrylonitrile Butadiene Styrene
C_D	Coefficient of Drag
CFF	Cross-flow Fan
C_L	Coefficient of Lift
CPU	Central Processing Unit
D	CFF Diameter
ESC	Electronic Speed Controller
F_x	Drag Force [N]
F_y	Lift Force [N]
HVAC	Heating, Ventilating, and Air Conditioning
PLA	Polylactic Acid
Prepreg	Pre-impregnated
ρ	Density [kg/m^3]
RPM	Revolutions Per Minute
TSR	Tip Speed Ratio ($TSR = U_\infty / \omega D$)
U_∞	Freestream Velocity, Always Only Horizontal [m/s]
U_{jet}	X Component of Jet Velocity [m/s]
V_{jet}	Y Component of Jet Velocity [m/s]
VTOL	Vertical Takeoff and Landing
ω	CFF Angular Velocity [rad/s]
y+	Dimensionless Wall Distance

THIS PAGE INTENTIONALLY LEFT BLANK

ACKNOWLEDGMENTS

I would like to thank several people for the time and support they have given me over the past year to help me accomplish this research:

Professor Garth Hobson, thank you for your complete support and confidence in me, and for giving me the opportunity to work on such a game-changing project. I cannot imagine any project I would have had more fun doing.

Professor Anthony Gannon, thank you for helping guide me through complicated Ansys variables and expressions and multirotor flight systems. You truly saved me lots of heart-ache.

John Gibson, thank you for taking the time to teach me how to use every tool I could possibly imagine, and then some—like the pistol-grip saw set. Your logical and common sense reasoning helped steer me away from lots of pitfalls.

Andrea Holmes, thank you for helping me with the electrical wiring codes.

Thanks to all of my family, especially my parents, for helping me reach my dreams, and especially to my Aunt Janet and Uncle Steve for being my home-away-from-home in California.

THIS PAGE INTENTIONALLY LEFT BLANK

I. INTRODUCTION

A. BACKGROUND

Cross-flow fan technology was patented by Paul Mortier in 1893 [1] and has been used commercially for the past century. Its rectangular profile and geometry make it ideal to fit inside a heating, ventilation, or air conditioning (HVAC) unit. The fan's axial rotation enables direct drive motors to attach and power the rotor while remaining outside the duct for easy maintenance access. Figure 1 shows a commercial cross-flow fan (CFF).

Figure 1. A commercial CFF used for cooling a central processing unit (CPU), from [2].

The aerospace community briefly considered cross-flow fan technology as a means of aircraft propulsion in the late 1960s [3]. However, the CFF has lower fan efficiencies than other means of propulsion [4]. Further yet, CFFs are not easily analyzed as steady-state devices in the same manner as propellers and gas turbines but require transient simulations which were not possible until the advent of inexpensive computing. Due to this, other propulsion systems such as turbo-prop and turbo-fan jet engines were developed much more rigorously than the CFF in the aerospace realm.

More recent research found that by embedding the CFF into a wing the overall propulsive efficiency can be greatly increased [4], and easily exceeds the sum of the components. This is due to the fundamental coupling between the wing and the CFF

which requires treating the embedded CFF-in-wing as a system rather than a combination of individual components. The CFF keeps the boundary layer attached over the top of the wing at greater angles of attack and provides circulation control, allowing for the use of thicker airfoils which would normally be too sensitive to stall. The thick wing geometry develops greater pressure differentials between the top and bottom and generates more lift than traditional wing cross-sectional profiles. Figure 2 shows a conceptual design from [4].

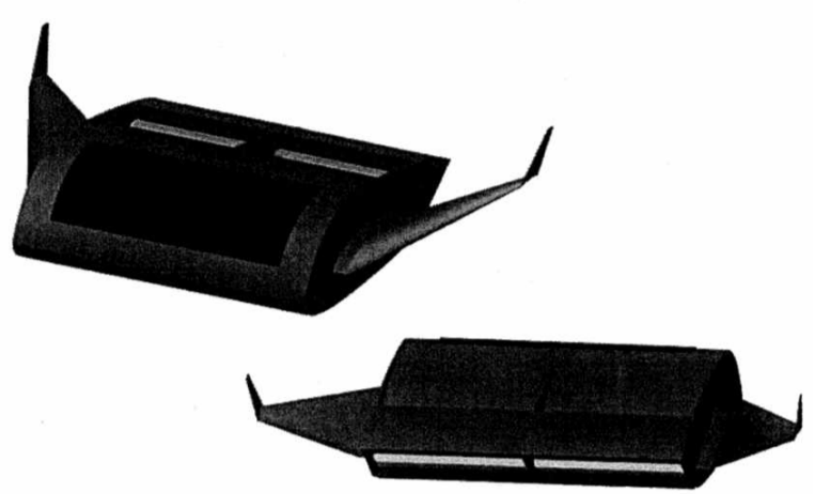

Figure 2. A CFF unmanned aerial vehicle conceptualized by Kummer, from [4].

While CFFs work well for propulsion in traditional aircraft, they can generate thrust coefficients great enough to lift via jet thrust alone. This has been demonstrated recently by Smitley [5] who developed a quad-rotor configuration using solely CFFs as propulsion. Figure 3 shows the vehicle setup.

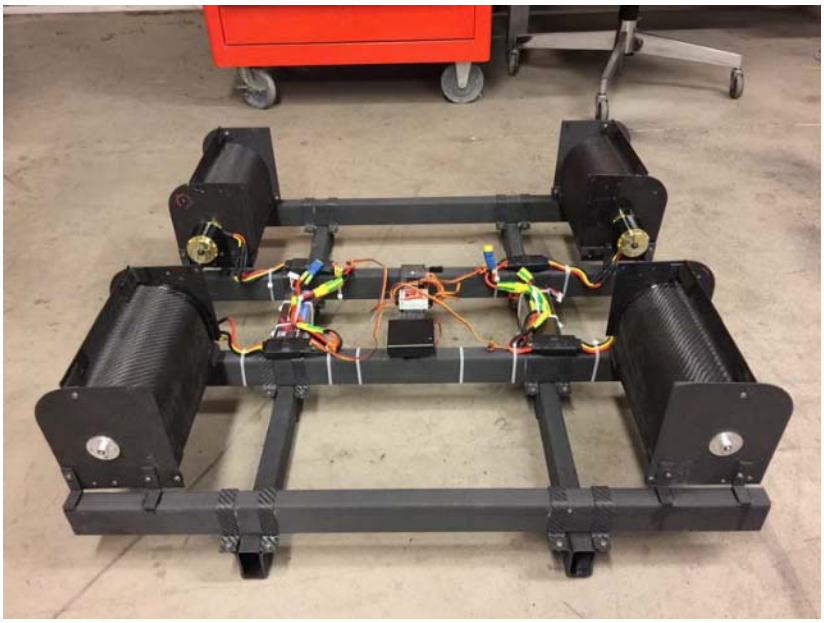

Figure 3. A CFF vehicle capable of controller stabilized vertical flight, from [5].

B. OVERVIEW

Transportation is vital in today's society. Common examples are bulk shipments across the ocean, next day air delivery, battlefield equipment airdrops, and mass people transport. Recently, companies such as Amazon have begun considering the use of multirotor flying vehicles to deliver packages. This enables for quicker deliveries, and deliveries to places where ground transport cannot reach. Figure 4 shows an air delivery vehicle proposed by Amazon for its Prime Air service.

Figure 4. Amazon octocopter, from [6].

Shortcomings of a multirotor aircraft are limited payload capacity and flight range in comparison to fixed wing aircraft. Concepts have been developed that combine a vertical takeoff and landing (VTOL) multirotor with traditional fixed wing flight. This allows both access to areas with small landing areas and a greater range. Figure 5 shows a more recent design for Amazon's Prime Air.

Figure 5. Amazon Prime Air delivery vehicle, from [6].

The Osprey (Figure 6) is a VTOL aircraft that transitions to horizontal flight using actuators that rotate its turboprops forward. The aircraft required years of research and development to produce materials and controllers that could handle the flight characteristics and in-flight reconfigurations. This could be avoided by an aircraft that changes between hovering and vertical flight by orientation only.

Figure 6. V-22 Osprey taking off vertically, from [7].

An embedded CFF style wing, or propulsive wing, coupled with a control stabilization system would enable an aircraft to hover and also fly vertically, generating lift from the wings, which would improve lift capacity, range, and maximum flight speed.

C. LITERATURE REVIEW

1. Embedded Crossflow Fan

Prandtl discussed improving wing lift by embedding a rotating cylinder within an airfoil [8], referencing experiments conducted by [9] which found lift coefficients (C_L) of 2.43 at 41.7º angle of attack (AOA) for a wing with a rotating cylinder embedded in its leading edge. Figure 7 shows an embedded rotating cylinder toward the front of a wing that was conceptualized by Prandtl [8].

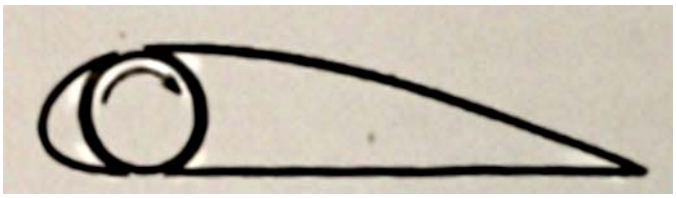

Figure 7. A rotating cylinder embedded in an airfoil conceptualized by Prandtl, from [8].

If the cylinder is a CFF and sucks air over the top and blows it out the bottom, it becomes more similar to a modern propulsive wing which controls the boundary layers by preventing flow detachment and provides circulation control about the wing. Figure 8 illustrates the difference between a propulsive wing with the CFF on and one with the CFF off.

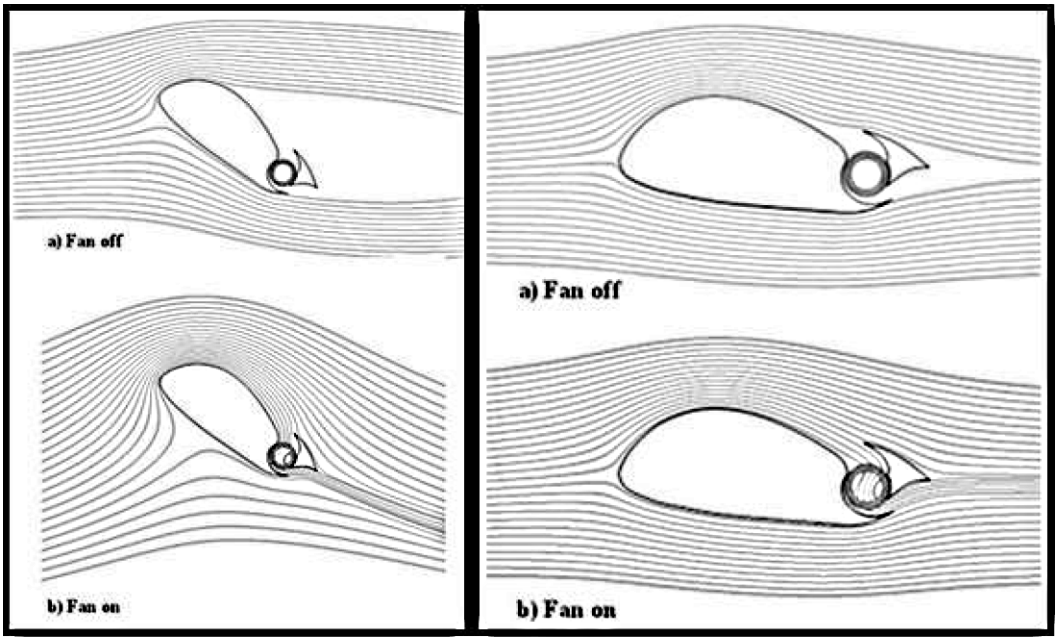

Figure 8. An example of boundary layer control over a propulsive wing, from [4].

2. Coefficient of Lift, Drag, and Tip Speed Ratio

An interesting matter to address is how a wing with embedded CFF should be characterized. If it is defined classically, the lift coefficient would be infinite in the case that the wing was hovering because there would be no airspeed. Additionally, the lift generated by the wing would change with CFF speed, but the classical lift coefficient definition would not account for this as is shown in Equation (1), where F_y is the lifting force, ρ is the fluid density, A is the planform area, and U_∞ is the freestream fluid velocity which is only in the horizontal x direction.

$$C_L = \frac{F_y}{\frac{1}{2}\rho A {U_\infty}^2} \tag{1}$$

In order to add the effects of CFF speed to the C_L, several methods have been proposed. One method proposed by [10] is to treat the lift added by the CFF the same as a jet flap, in which case [11] suggests the C_L be a combination of the wing C_L and jet flap C_L. Another option is to use the classical C_L form with a velocity that is representative of both the freestream velocity and the CFF rotational speed. This is the case with Equation (2), which uses the average of the freestream velocity (U_∞) and the magnitude of the outlet jet velocity, which uses the x component of the jet velocity (U_{jet}) and the y component (V_{jet}).

$$C_L = \frac{F_y}{\frac{1}{2}\rho A(\frac{U_\infty + \sqrt{{U_{jet}}^2 + {V_{jet}}^2}}{2})^2} \tag{2}$$

The coefficient of drag (C_D) can be calculated similarly using Equation (3), where F_x is the drag force.

$$C_D = \frac{F_x}{\frac{1}{2}\rho A(\frac{U_\infty + \sqrt{{U_{jet}}^2 + {V_{jet}}^2}}{2})^2} \tag{3}$$

Another component that can be used to non-dimensionalize the freestream and CFF speeds is tip-speed-ratio (TSR), which is defined in Equation (4) where ω is CFF angular

velocity and D is the CFF's diameter. TSR is used in CFF-wing characterization by [12], [13], and [14] who called it a fan flow coefficient.

$$TSR = \frac{U_\infty}{\omega D} \tag{4}$$

D. OBJECTIVES

The goals of this research were threefold. First, to develop a wing with an embedded CFF with large lift coefficients. Second, to manufacture the wing design using molds that were 3D printed. Third, to assemble the wings in a flyable configuration with all wings facing forward, as opposed to Smitley's design that was a more traditional quadcopter configuration concept [5].

1. Heavy Lifting Wing Design

SolidWorks and Ansys were used to develop and characterize a propulsive wing geometry. The resulting wing chosen was rather thick to enable a CFF to be embedded and to generate high lift for a high payload capacity aircraft.

2. 3D Printed Mold Wing Fabrication

Manufactured carbon fiber wings were laid up using molds printed with a 3D printer. Print material selection was based on filament glass transition temperature and printability.

3. Forward Facing CFF Vehicle Configuration Capable of Vertical and Horizontal Takeoff and Landing

The propulsive wing assemblies were configured into a quad-shape arrangement with all fans facing forward, which was counter to prior configurations that used symmetry to increase stability. This aircraft was controlled by a commercial multirotor aircraft flight controller and took off and hovered similar to a quad-rotor, but ultimately will include an undercarriage and be able to roll for a horizontal takeoff. This will enable both vertical and horizontal takeoff and landing.

II. DESIGN

A. FIRST-, SECOND-, THIRD- AND FOURTH-GENERATION VEHICLE DESIGN

Initial vehicle designs encompassed everything from tethered uncontrolled flight to untethered controlled flight and were motivated by developing an aircraft platform that was capable of VTOL, efficient hover, and transition to efficient forward flight. The first-generation was uncontrolled and built to demonstrate the CFF's ability to provide vertical lift. The design had a thrust to weight ratio of 1.79 [15]. Figure 9 shows the design.

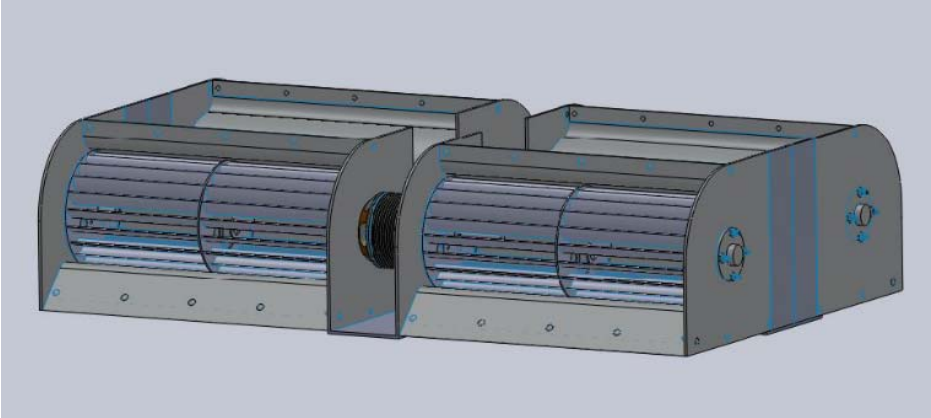

Figure 9. First-generation vehicle design, from [15].

The second-generation design added two addition motors so each fan was powered separately, increased footprint and structural rigidity, and added a controller to enable stabilization [5]. Figure 10 shows the design.

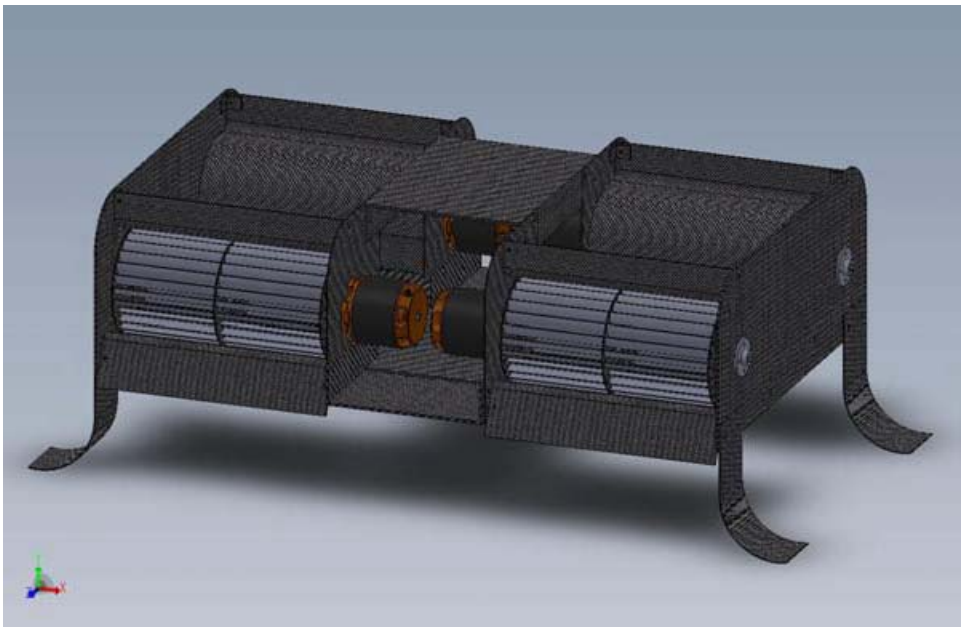

Figure 10. Second-generation vehicle design, from [5].

The third-generation improved on manufacturing, decreasing vehicle weight, but had poor CFF placement resulting in no yaw control. Figure 11 shows the vehicle. This design was quickly modified into the fourth generation, Figure 12, which had the rear CFFs facing backward so as to enable yaw control and improve pitch control through symmetry.

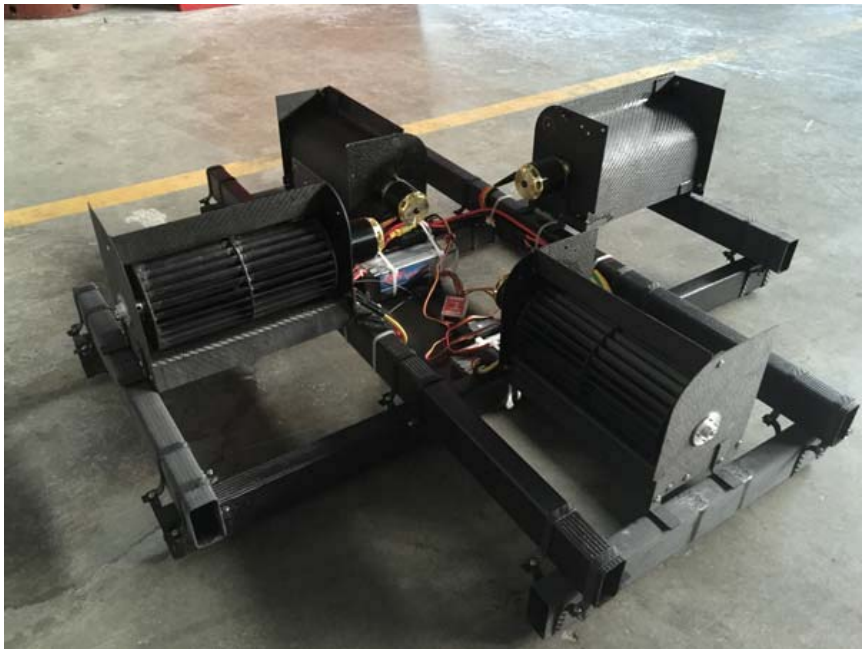

Figure 11. Third-generation vehicle design, from [5].

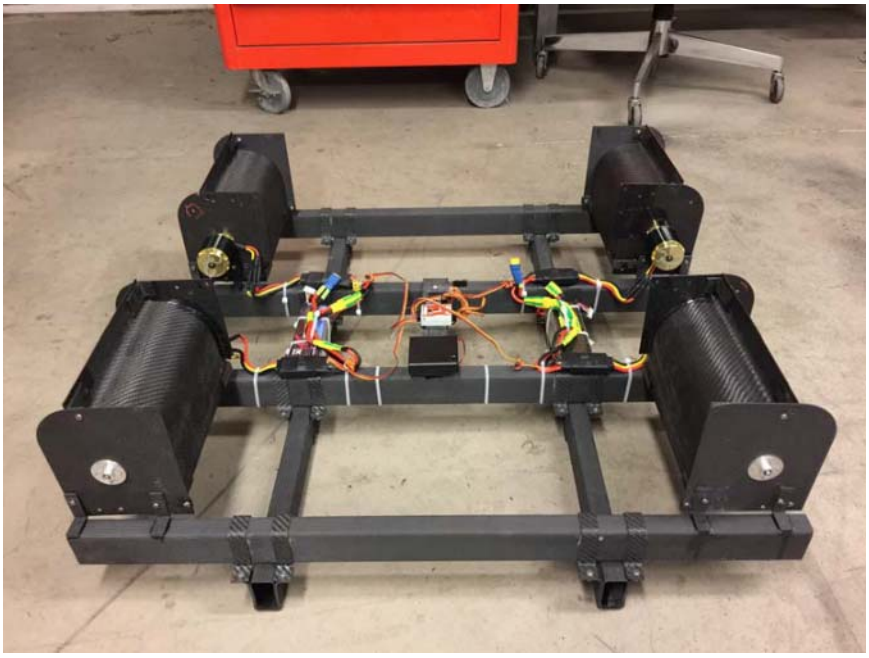

Figure 12. Fourth-generation vehicle design, from [5].

B. FIFTH-GENERATION VEHICLE DESIGN

The fifth generation had several large design modifications. The CFFs were embedded into an airfoil, which fundamentally coupled the CFF and wing in a manner which generated more lift than possible by solely summing the components. Additionally, all the wing assemblies were aligned in the same direction as opposed to previous generations that had mirrored geometry for better stability. Aiming all the CFFs and their wing assemblies in the same direction was to favor forward flight. In order to support the preferential forward flight and wing assemblies, a larger frame was used to increase stability of the system by increasing the moment of inertia and moment arm of each wing. Finally, the configuration was slightly longer than it was wide to increase pitch stability.

1. Airfoil Design

Airfoil design is part science and part design craftsmanship. The wing must function properly with the desired characteristics, but it should also appear aerodynamic which is usually visually appealing as is the work of a craftsman. In the case of an airfoil designed purely for research purposes, the scientifically well designed airfoil will often look correct, hence the craftsmanship and art in airfoil design.

The airfoil needed in this case was one capable of accommodating an internal CFF. The airfoil needed to be thick enough to fit a CFF but also possess a geometry that would enable the smooth transition of air flowing over the top of the wing to the CFF and out the back. The airfoil geometry chosen was the Gottingen 570 airfoil, shown in Figure 13, primarily because it possessed the desired geometrical characteristics and had been successfully used by Kummer [4] in propulsive wing design.

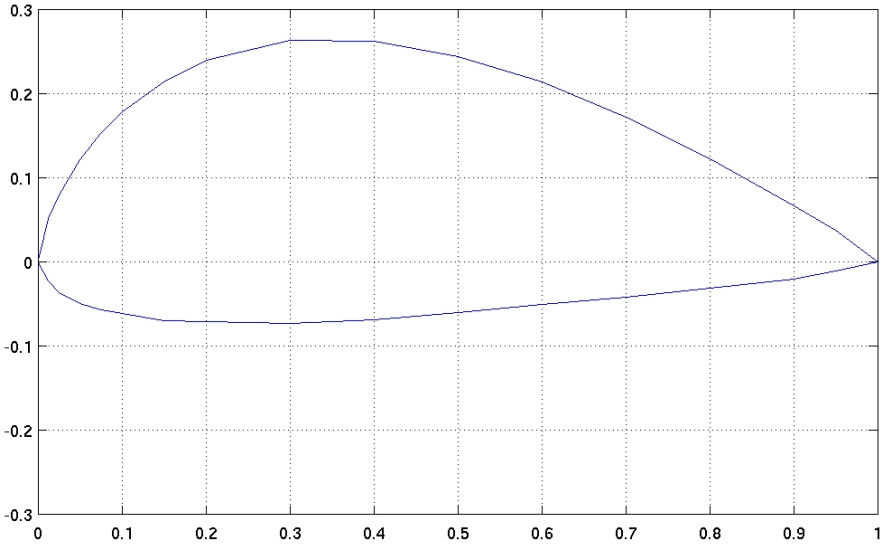

Figure 13. Gottingen 570 airfoil geometry, from [16].

Kummer used a large geometry, embedding the CFF in the trailing edge of the wing as shown in Figure 14, which has the wing at a 40º AOA. This was possible because the wing was meant to fly horizontally and was thus able to rely heavily on wing-lift for flight.

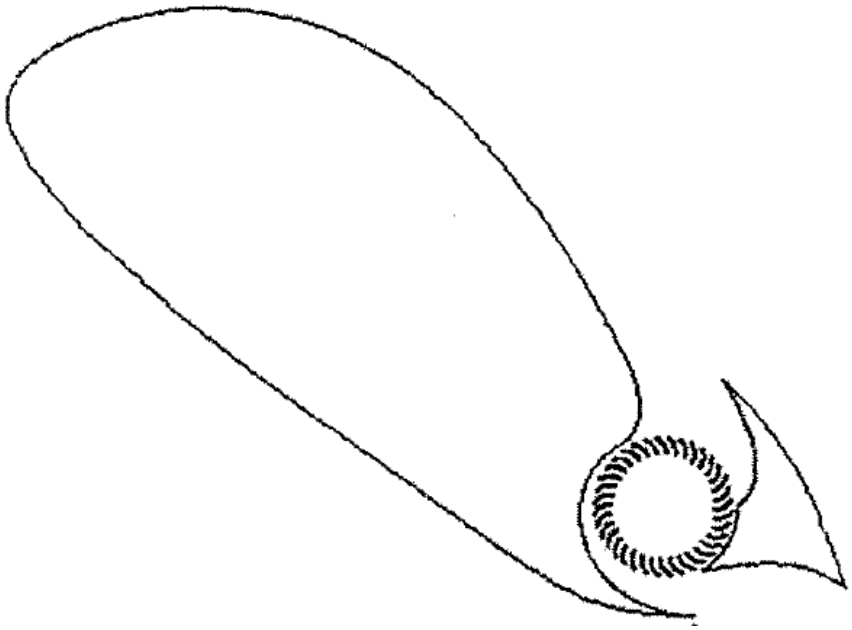

Figure 14. Kummer's airfoil based on the Gottingen 570, from [4].

Alternatively, the wing developed here needed to be light enough to hover. Ideally the airfoil design would generate lift while hovering to decrease the required jet thrust. In order to accomplish this, a 0.5 m (19.7 in) wing chord was used in conjunction with a 0.102 m (4 in) diameter CFF and a maximum wing thickness of 0.169 m (6.6 in). Using a MATLAB script, Appendix A, the Gottingen 570 geometry was read from [16] to SolidWorks. The CFF geometry was added and the airfoil design changed to accommodate the CFF. The CFF works best with a larger intake area than exit area, which maximizes the thrust produced. This was considered when designing the airfoil. Initial Ansys simulations found the wing changed the air direction by about 30º, so the CFF outlet geometry was aimed a further 30º downward, ensuring the wing would hover at an AOA less than 90º. Figure 15 shows the final modified Gottingen 570 airfoil design.

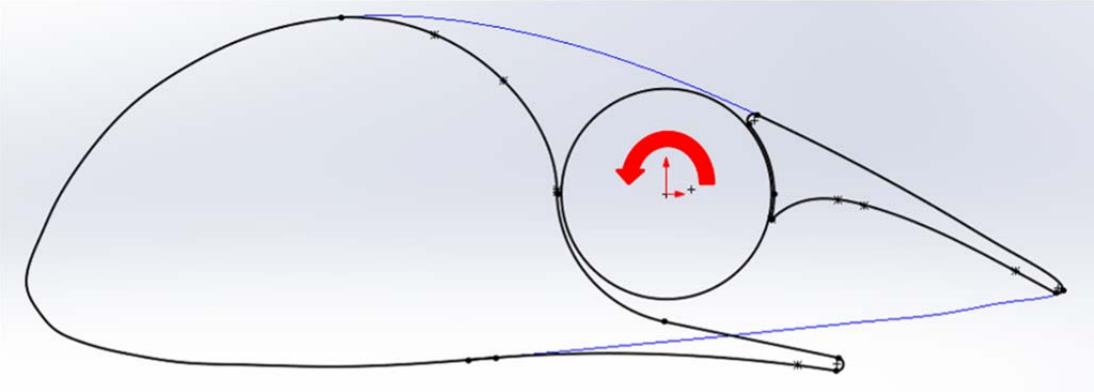

Figure 15. The modified Gottingen 570 final wing design with a chord length of 0.5 m.

2. 2D–Ansys Simulation

SolidWorks geometry was imported into Ansys CFX module as a 1 mm thick section for 2D simulation. The simulation was considered 2D to simplify the transient setup. Additionally, for a sufficiently long wing the flow would be 2D. In order to parametrize AOA the wing was placed in a circle 8 m (26.2 ft) in diameter with the CFF centered. The circle was then set inside a rectangular geometry with overall dimensions of 10 m x 10 m (32.8 ft x 32.8 ft). This enabled the AOA to be easily changed and

remeshed without extensive Ansys setup each time AOA was modified. Figure 16 shows the geometry schematic and Appendix B contains the Ansys block diagram.

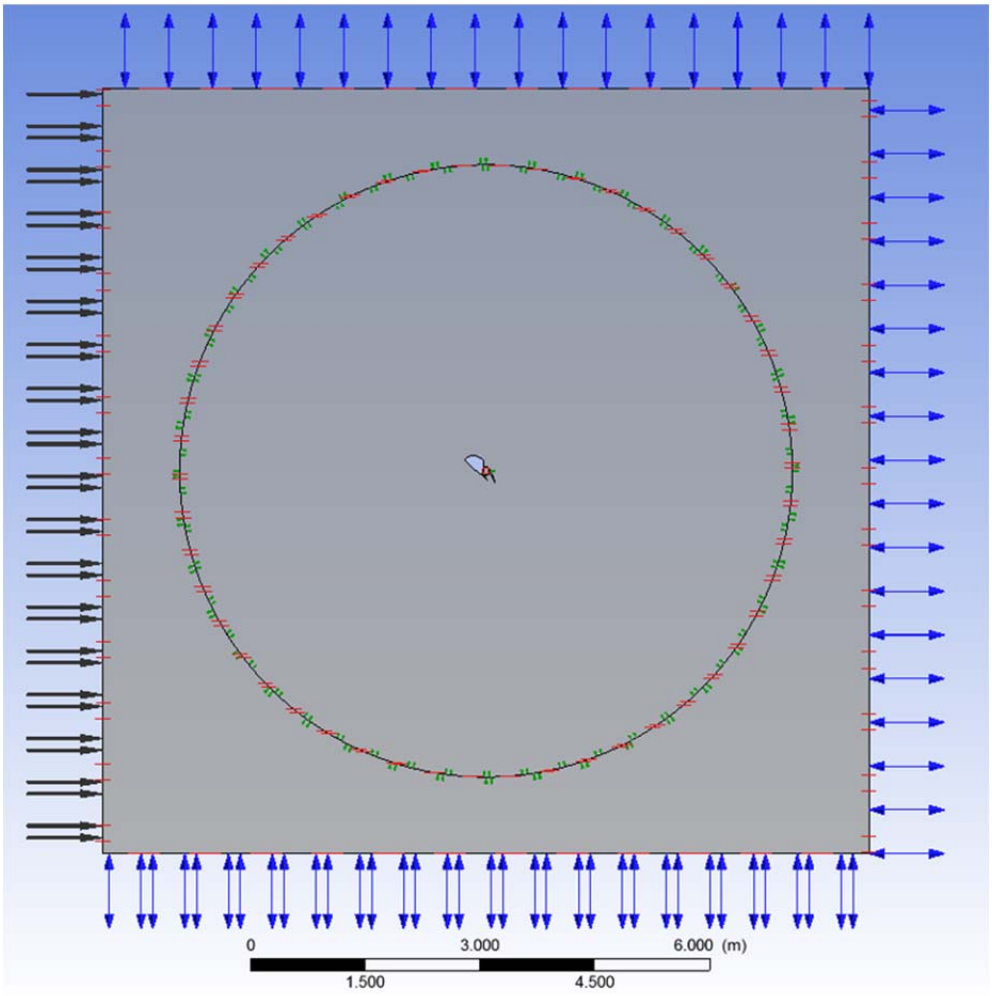

Figure 16. 2D simulation domain with rotating geometry for AOA variation, shown with the wing at 45º.

A mesh with 66,358 elements and 141,180 nodes was used for the 2D simulation over the wing cross section. Inflation layers and edge sizings enabled a manageable number of nodes and elements while keeping the average dimensionless wall distance (y+) values, defined in White [17], under 18 on the airfoil and 31 on the CFF blades. The inflation layers were set on the symmetry face with a starting point of the airfoil edge. A sweep method with a single cell division was used over the entire domain. The rotating

interface between the CFF and airfoil was set with 600 cell divisions on either side. This helped ensure conservation over the sliding mesh interface during simulation. Figure 17 shows the sliding interface and airfoil inflation layers.

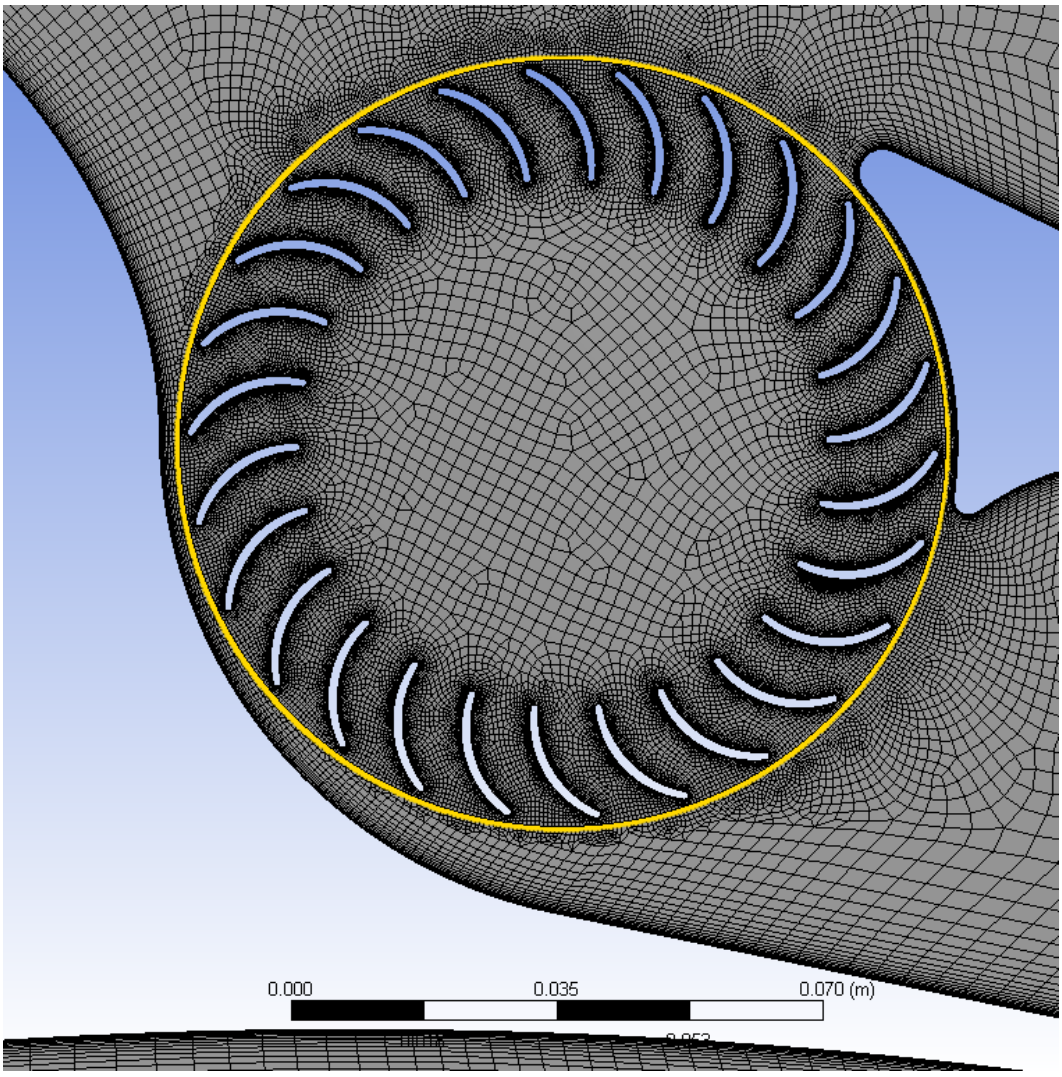

Figure 17. The sliding mesh between the CFF and airfoil is shown in yellow and rotates counter-clockwise.

The Ansys CFX simulation was run with 1º of CFF rotation per time-step and until torque, lift, and drag stabilized. This normally took between 5 and 15 rotations of the CFF, but took up to 25 rotations for the higher AOAs that had large freestream airspeeds. Additionally, the domain was initiated with the prescribed freestream velocity.

Runs with no freestream airspeed used to simulate hover found that the propulsive wing design would hover at an AOA of 36º. Figure 18 shows solution with streamlines for a TSR of 0.15 and AOA of 40º.

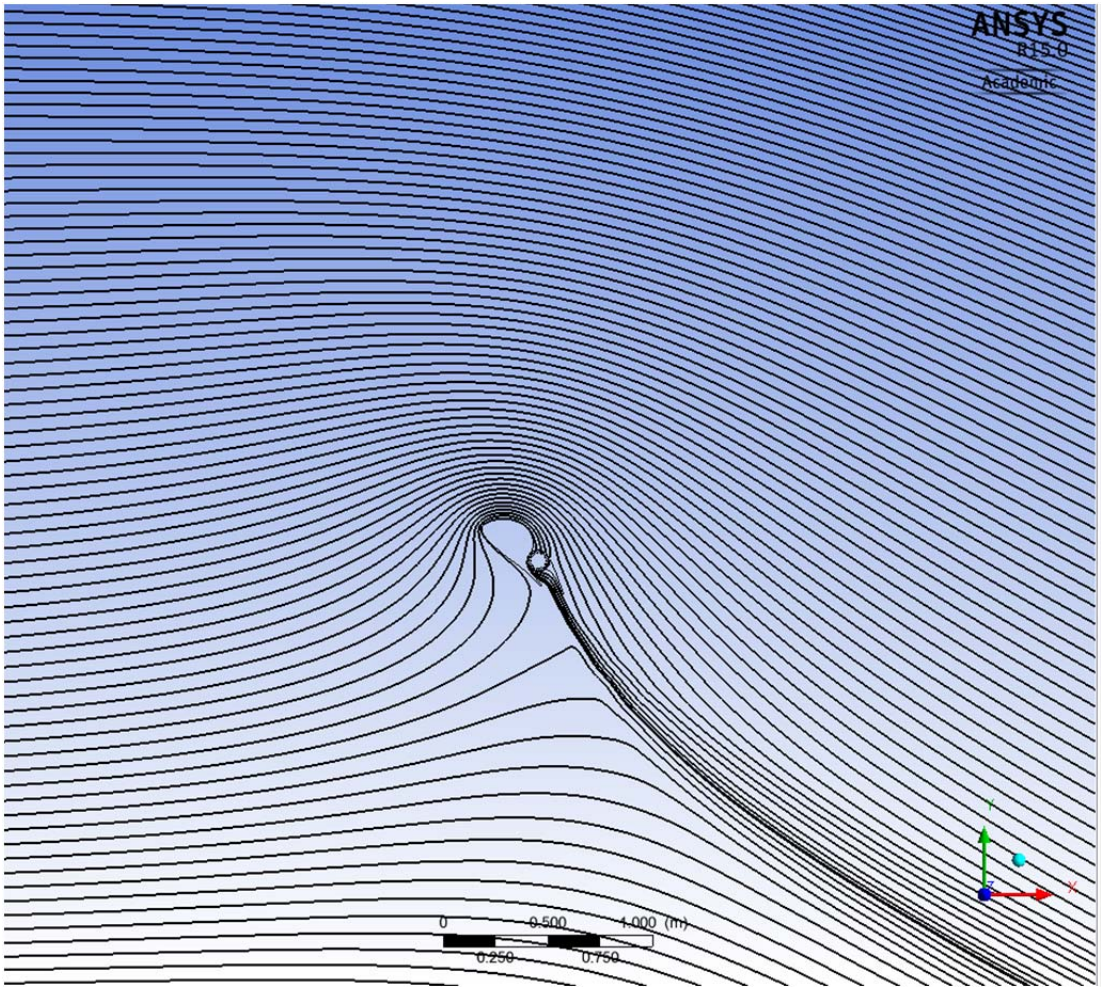

Figure 18. Streamlines from a simulation with a TSR of 0.15 and AOA of 40º.

3. 3D–Ansys Simulation

In order to better understand the propulsive wing characteristics, 3D steady-state simulations were conducted using prescribed CFF inlet and outlet mean velocities. The 2D simulations were used to determine these velocities over a range of TSRs for a rotor speed of 8000 revolutions per minute (RPM) and 6000 RPM. Figure 19 shows the mean velocities at the inlet and outlet (jet) used in the 3D steady-state simulations.

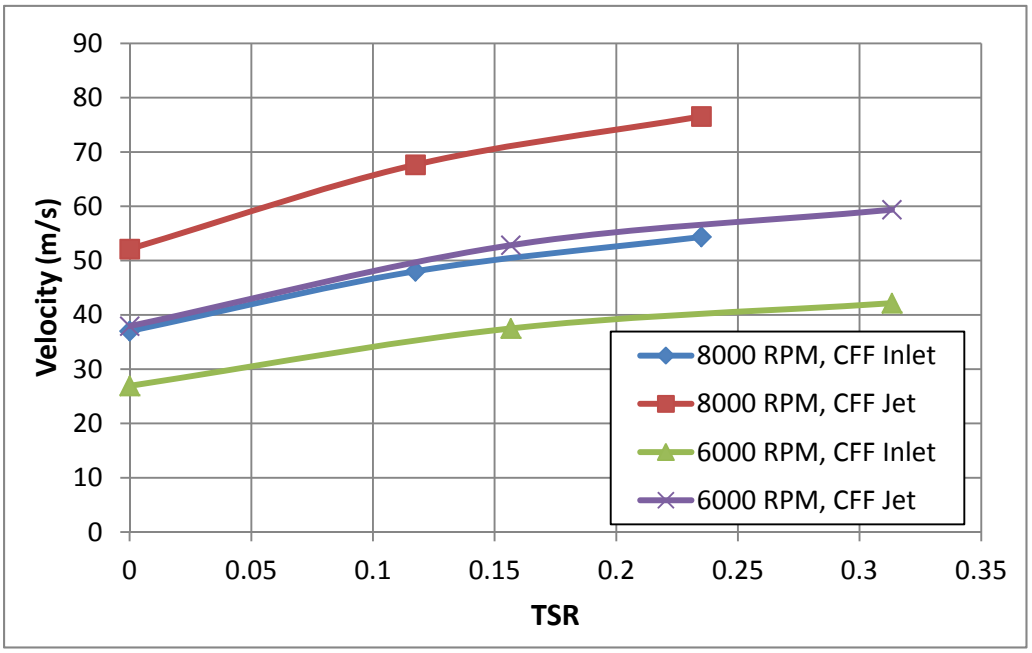

Figure 19. 2D inlet and jet velocity simulation data used for 3D simulations.

A steady-state quad configuration consisting of four wing assemblies and no connecting struts was simulated using Ansys CFX. Figure 20 shows the configuration used. The angles were set based on the 2D simulations so that the aircraft would fly in horizontal flight as shown and hover lying flat so all four wings aligned horizontally with AOAs of 36º.

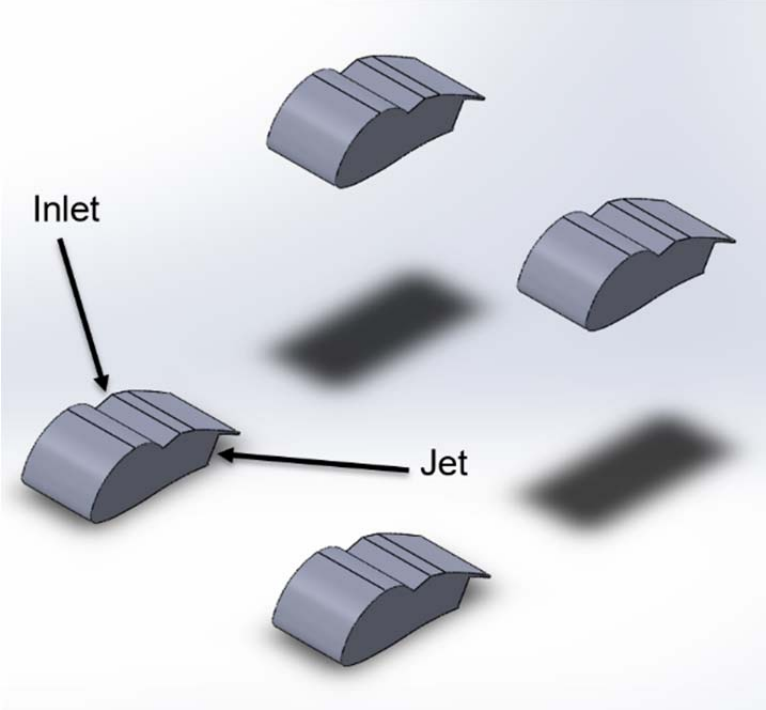

Figure 20. Configuration for 3D simulation.

The simulations showed that the flow over the wings was 3D and generated wingtip vorticities. Figure 21 shows entrained streamlines along a plane 1.27 cm (0.5 in) past the end of the wing. The vortices can been seen beginning as they curl up from the bottom around the sides and spin off the back trailing edges of the wings. The predicted hover angle was 56º.

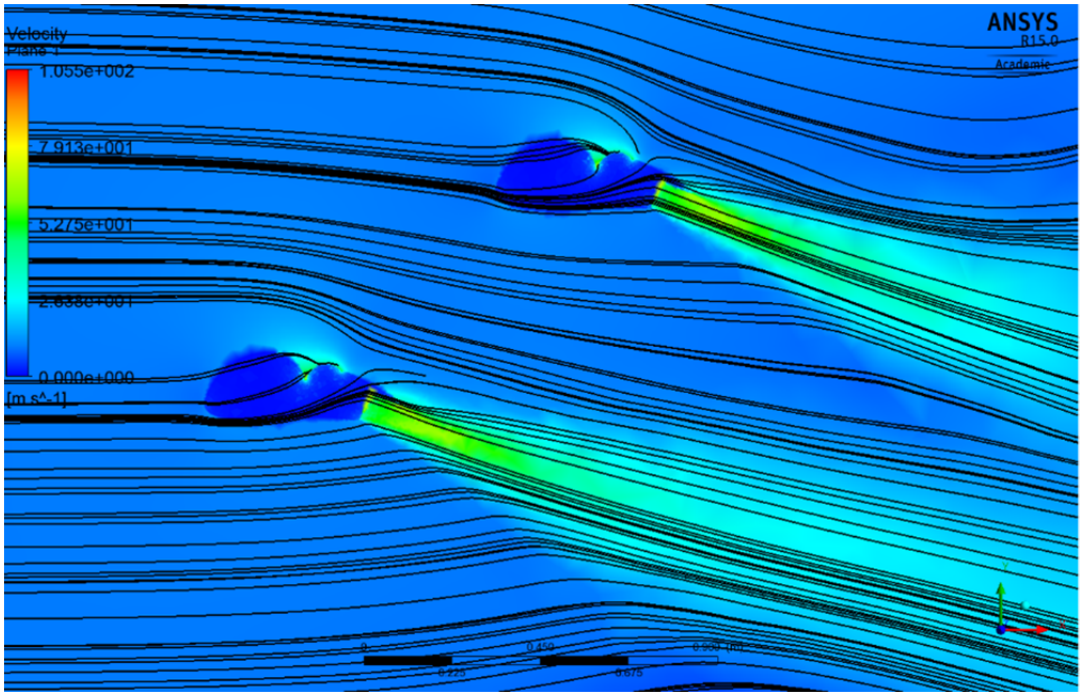

Figure 21. Wingtip effects on a plane 1.27 cm (0.5 in) past end of wings.

4. 2D and 3D Simulation Comparison and Consequences

The 2D and 3D simulations varied in two primary manners. First the hover angle, and second, the lift generated per wing while hovering. Lift calculations were conducted assuming 20.3 cm (8 in) long CFFs in 22.9 cm (9 in) wide airfoils. The predicted hover angle for the 2D simulation was 36º while the 3D simulations predicted a hover angle of 56º. The lift generated per wing while hovering was predicted to be 10.5 kg (23.1 lbf) by the 2D simulations while the 3D simulations predicted 9.0 kg (19.9 lbf) of lift. The differences are likely due to the addition of the wingtip effects in the 3D simulations, which would tend to degrade wing performance. For both the 2D and 3D simulations, the wing would not need to rotate a full 90º to transition from hovering to conventional flight. This was advantageous because the wing would not need to have as great of motion in the case that it was actuated, or for fixed wings, the aircraft would not need to reach as great of angles which would allow for better passenger comfort or simpler cargo management.

5. Wing Characterization, Lift, Drag, and Power

The simulation results from the 2D Ansys simulations were used to develop C_L versus AOA plots. C_L was calculated using the averaged U_∞ and U_{jet} which found that C_L did not depend heavily on CFF speed but rather on airspeed as Figure 22 shows. This allowed the wing to be parameterized using TSR.

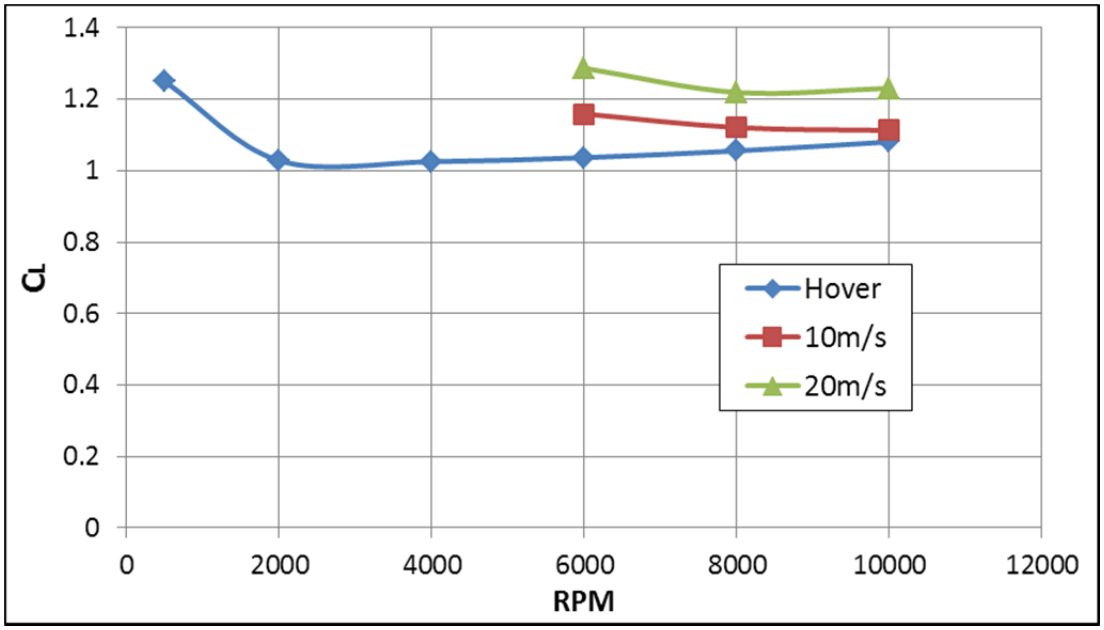

Figure 22. C_L at varied TSRs remains constant with CFF RPM change.

Calculating lift and drag on the wing for C_L and C_D was accomplished by using the x and y force components on the wing surface given directly by Ansys Post. Calculating the thrust from the CFF was not as simple. The thrust was calculated by determining the change in momentum between the inlet and jet on the airfoil. A user variable velDOTn, an array of scalar values, was defined in Ansys CFX Post as Equation (5), where $\underline{\boldsymbol{U}}$ is an array of the x, y, and z velocity components of the fluid at each mesh point and $\widehat{\boldsymbol{N}}$ is an array of x, y, and z normal components at each mesh point. The flow was 2D but the z component was still needed by Ansys CFX in order to run.

$$velDOTn = \underline{\boldsymbol{U}} \bullet \widehat{\boldsymbol{N}} \tag{5}$$

Then, also in Ansys CFX Post, the rotor thrust was calculated using the expressions given by Equations (6) and (7) over the CFF inlet and outlet jet. All the Ansys CFX variables, expressions, and user defined codes are included in Appendix C.

$$RotorThrustX = -\rho \sum_i \left(\left(U_{jet,i} - U_\infty \right) \; velDOTn_i \; A_{jet,i} \right) \tag{6}$$

$$RotorThrustY = -\rho \sum_i \left(V_{jet,i} \; velDOTn_i \; A_{jet,i} \right) \tag{7}$$

Using these, C_L and C_D versus AOA plots were developed for a range of TSR values. TSR was varied between zero and infinity, where zero was when the propulsive wing was hovering and infinity was when it was gliding with the CFF turned off. Figure 23 shows the C_L plot and Figure 24 shows the C_D plot. The optimum AOA for maximum lift was 60º for a TSR of 0.05 and decreased as TSR increased. This corresponded to increasing airspeed, which was ideal because it represented the desired flight orientation rotation between hovering and forward flight. Note that in the C_D plot negative values of C_D represent thrust and positive values represent drag.

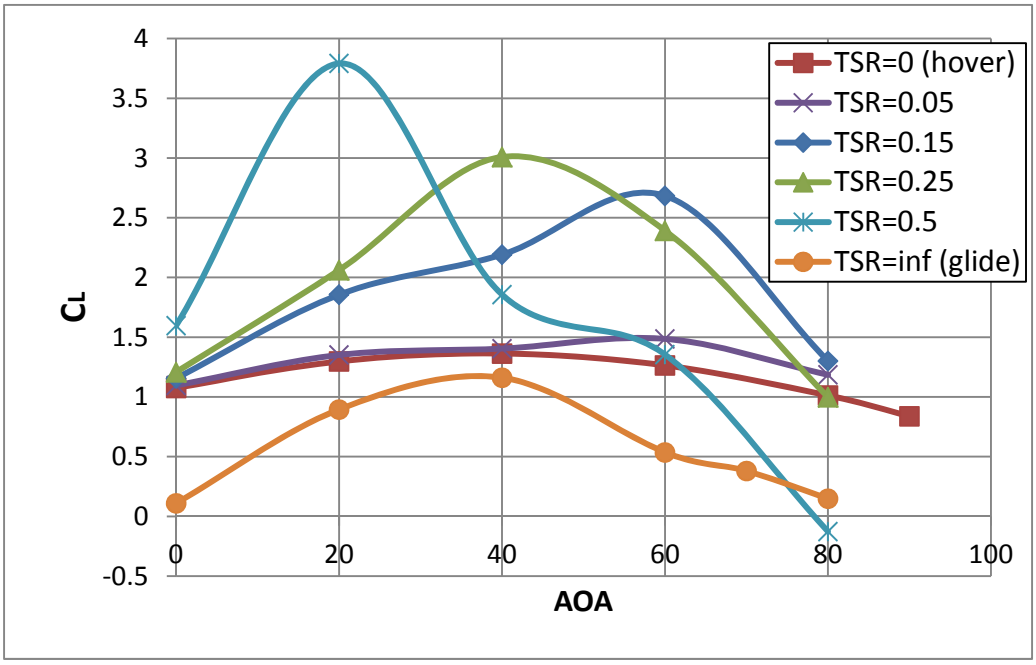

Figure 23. Simulated C_L versus AOA over a range of TSR values.

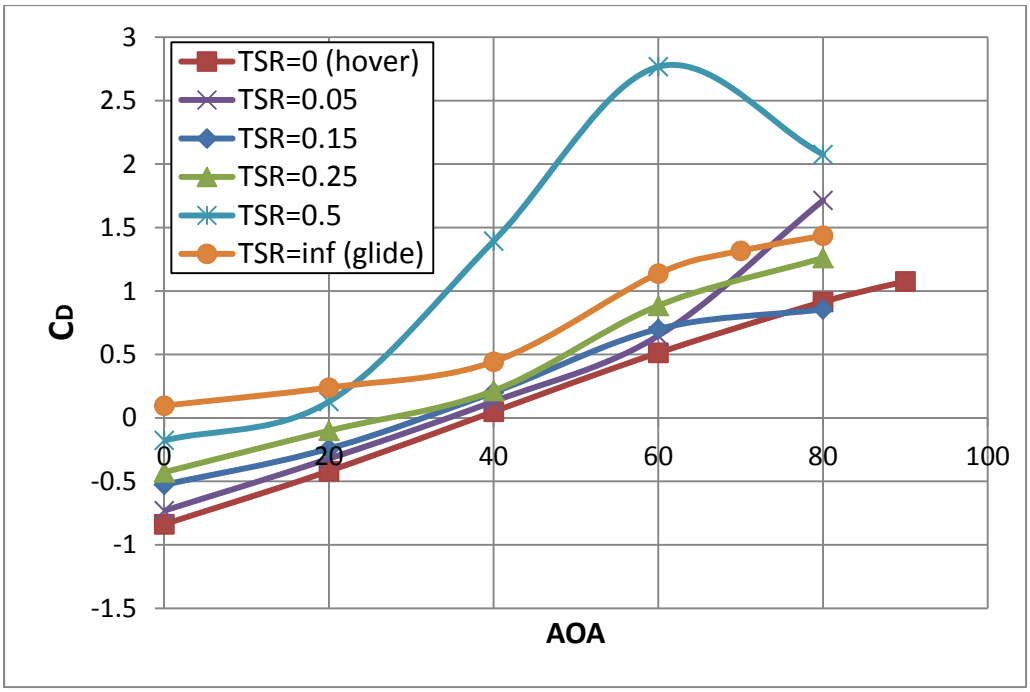

Figure 24. Simulated C_D versus AOA over a range of TSR values.

Table 1 shows the lift generated by the airfoil and CFF for comparison at hover and for accelerating conditions. Simulations from 20º and 40º were extrapolated out to reflect the hover angle of 36º. The coupling of the airfoil with the CFF enabled the airfoil to generate large percentages of the overall lift such that 56% of the total lift was generated by the airfoil and 44% by the CFF.

Table 1. Airfoil and CFF lift comparison.

Flight Condition	**AOA**	**Airfoil Lift**		**CFF Lift**		**Total Lift**
	(º)	(N/m)	(%)	(N/m)	(%)	(N/m)
Forward Acceleration	20	286.0	62.6	171.0	37.4	457.0
Hover	36	267.0	56.2	208.3	43.8	475.3
Backward Acceleration	40	262.3	54.6	217.7	45.4	479.9

Power versus RPM was calculated and plotted in Figure 25 for a 20.3 cm (8 in) wing and CFF in hover conditions with an AOA of 36º. Power was calculated by multiplying torque with RPM. The power curve fell slightly lower than what Martin [2] found.

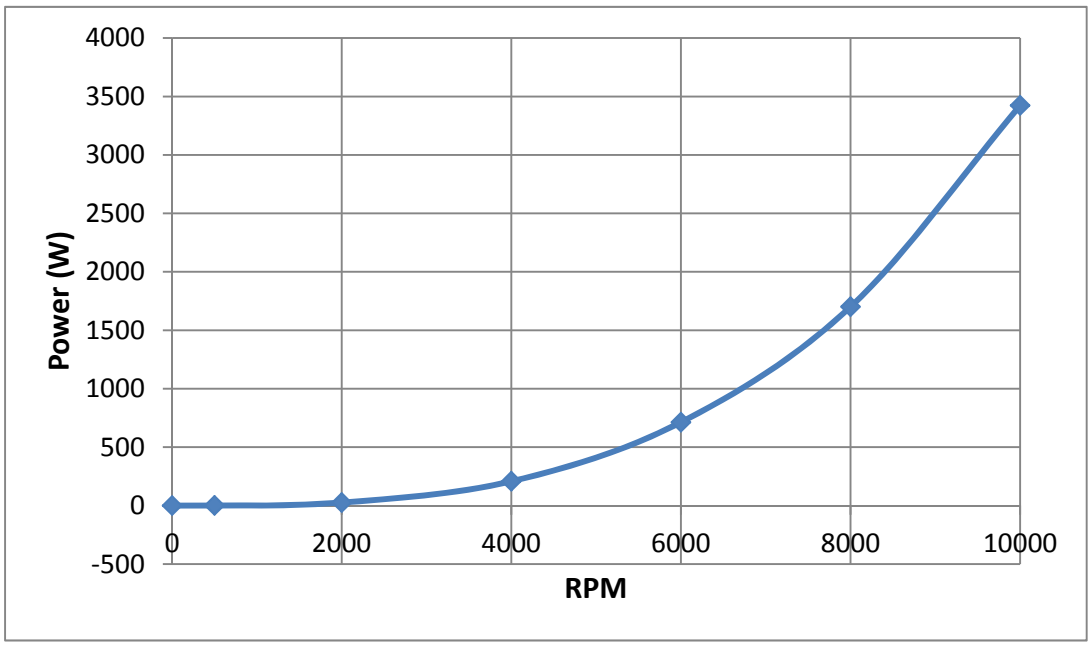

Figure 25. Simulated power versus RPM at the hover angle of 36º and no airspeed.

6. Flight Development Process

The fifth-generation vehicle went through several configuration changes throughout the construction process in order to improve stability and control. The controller's performance greatly improved once the center of mass was lowered and centralized and corresponded to the main controller location. Figure 26 shows an initial conceptual design where each wing assembly was 22.9 cm (9 in) wide and held an embedded 20.3 cm (8 in) long CFF. Figures 27 and 28 show the intended hover and horizontal flight configurations, respectively.

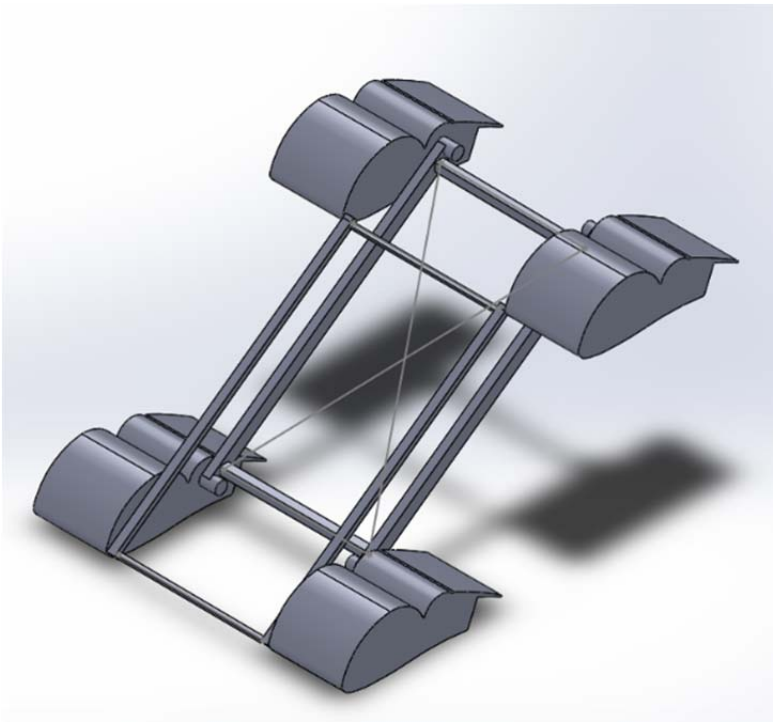

Figure 26. An initial conceptual configuration.

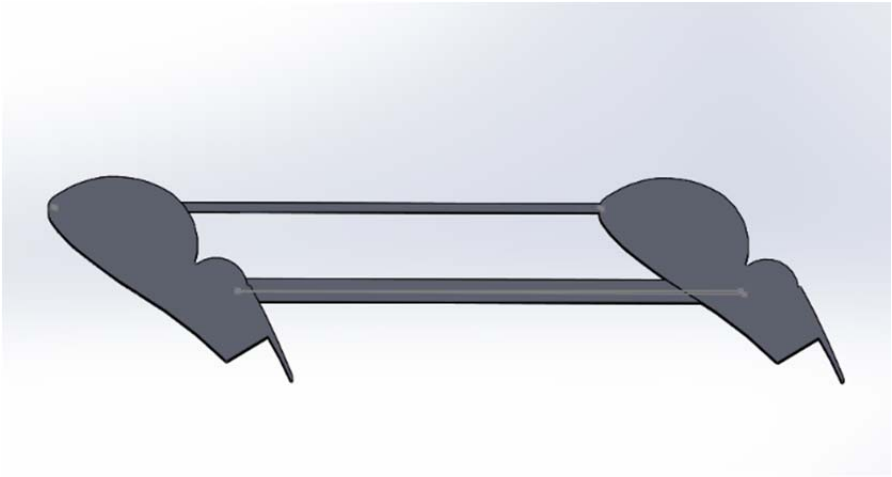

Figure 27. Aircraft hover orientation.

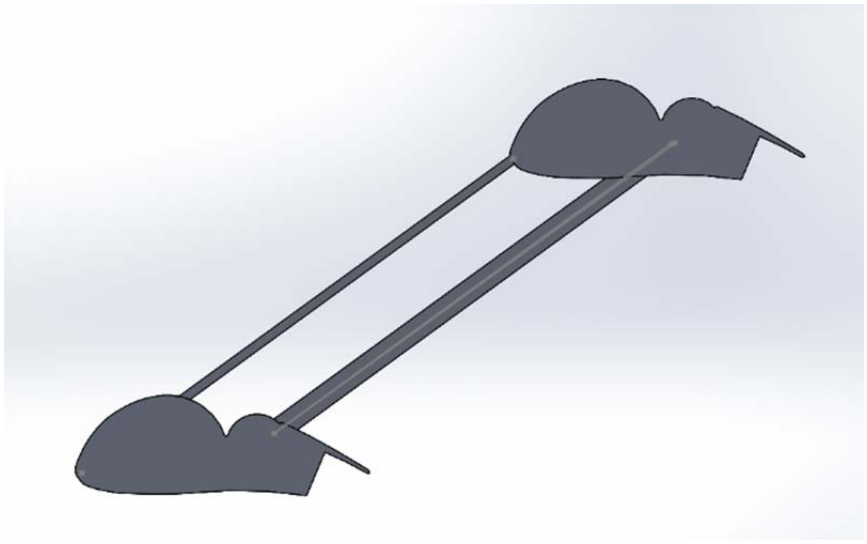

Figure 28. Aircraft horizontal flight orientation.

a. Mark I

The aircraft geometry was set according to the hover angle indicated by the 2D Ansys simulations. The front wings were set at a 40º AOA and the back wings at a 30º AOA. Steeper AOAs were used for the front wings in order to stabilize the vehicle similar to canards which stall first, and thus prevented the vehicle from reaching a too great of AOA. Additionally, the 10º difference between the front and back wings was to increase pitch stability and enabled the controller to have yaw control. The controller used was intended for a quad-rotor with inward spinning front rotors coupled across the diagonals. When yawing, the controller increased rotor speed on the rotor in the front corner closest to the direction of turn and the corresponding rotor across the diagonal and decreased the other two rotors to maintain the same vertical position. The same ability of yawing by increased and decreased CFF speed was maintained by setting the front wing assemblies at a slightly greater AOA than the back wing assemblies. Figure 29 shows the Mark I configuration prior to wiring. Ansys simulations predicted it would hover close to a horizontal vehicle orientation, but testing found the vehicle actually hovered at a positive angle.

Figure 29. Fifth-generation, Mark I prior to wiring.

b. Mark II

The Mark II configuration, Figure 30, included the addition of landing gear that held the vehicle at a positive angle to enable a balanced takeoff. Increased vehicle AOA put the front and back wings at an AOA of 76º and 66º, respectively. Wheels were added to cushion the landing and allow the aircraft to make a rolling takeoff. This configuration was flyable, but unable to hover stably and tended toward forward flight.

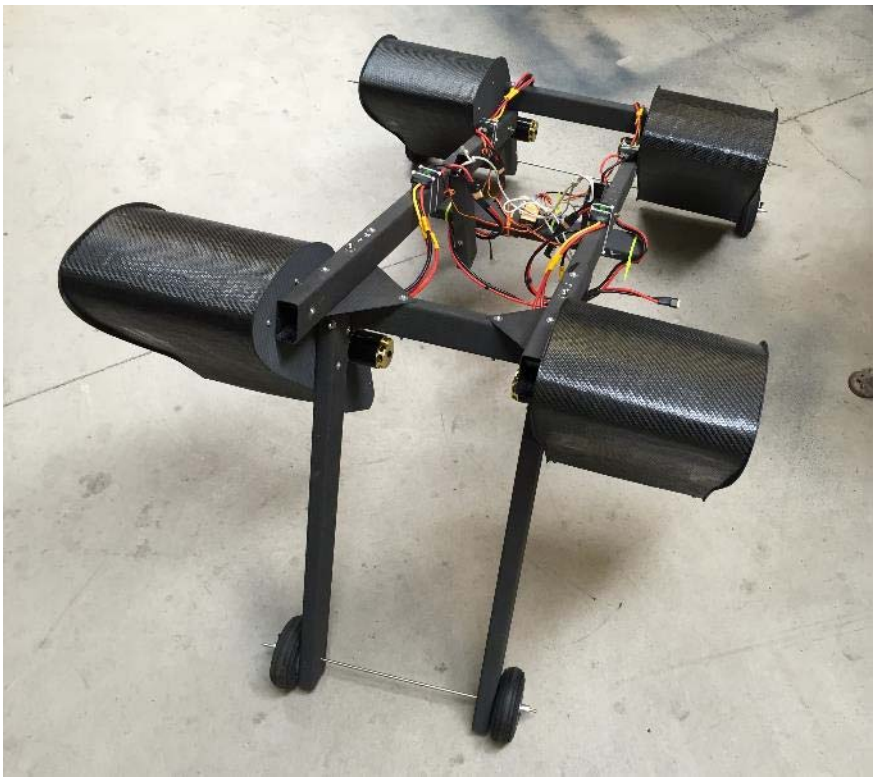

Figure 30. Fifth-generation, Mark II.

c. Mark III

The Mark III configuration, Figure 31, changed the front and back wing assemblies to AOAs of 85º and 75º, respectively, in order to decrease the tendency toward forward flight. The change also encompassed a vehicle reorientation so that it would rest horizontally on the ground. While hover ability greatly improved, the center of mass was high due to battery placement. Additionally, the controller was about 0.15 m (6 in) above the center of mass. Both of these caused erratic vehicle flight that required great pilot skill to control.

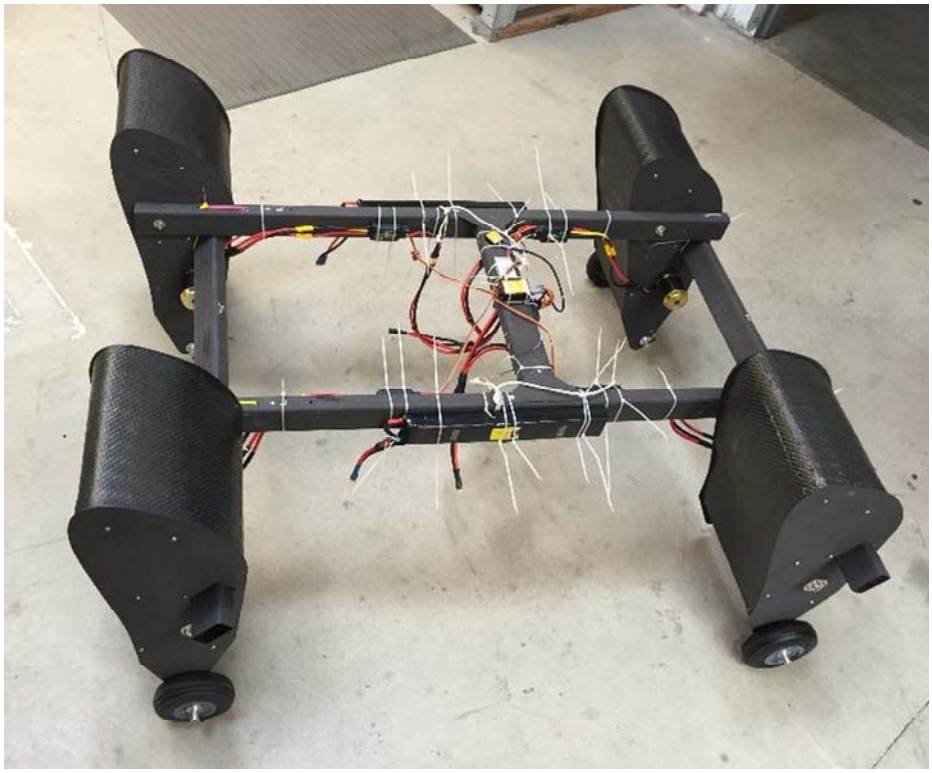

Figure 31. Fifth-generation, Mark III.

d. Mark IV

The Mark IV configuration, Figure 32, had a lower center of mass, improved rigidity, a lower overall mass, and a controller placement centered on the center of mass. Additionally, the back wing assemblies' AOA was decreased to 65º based on the hover angle of the previous configuration, which improved pitch stability. The wheels were removed and replaced with landing struts that weighed 80% less (0.2 kg versus 1.0 kg) with the assumption that the current vehicle would land vertically. This configuration hovered very steadily with about a 15º forward tilt, and could easily take off and land. This tilt gave the wings AOAs of 70º in the front and 50º in the back, which was very close to the 56º hover AOA predicted by the 3D Ansys CFX simulations. Figure 33 shows the fifth configuration in its intended forward flight orientation. The weight distribution of all materials used is given in Table 2. Aircraft dimensions were 1.2 m (4 ft) long, 0.91 m (3 ft) wide, and 0.61 m (2 ft) high, weighing 10 kg (21 lbs) with batteries.

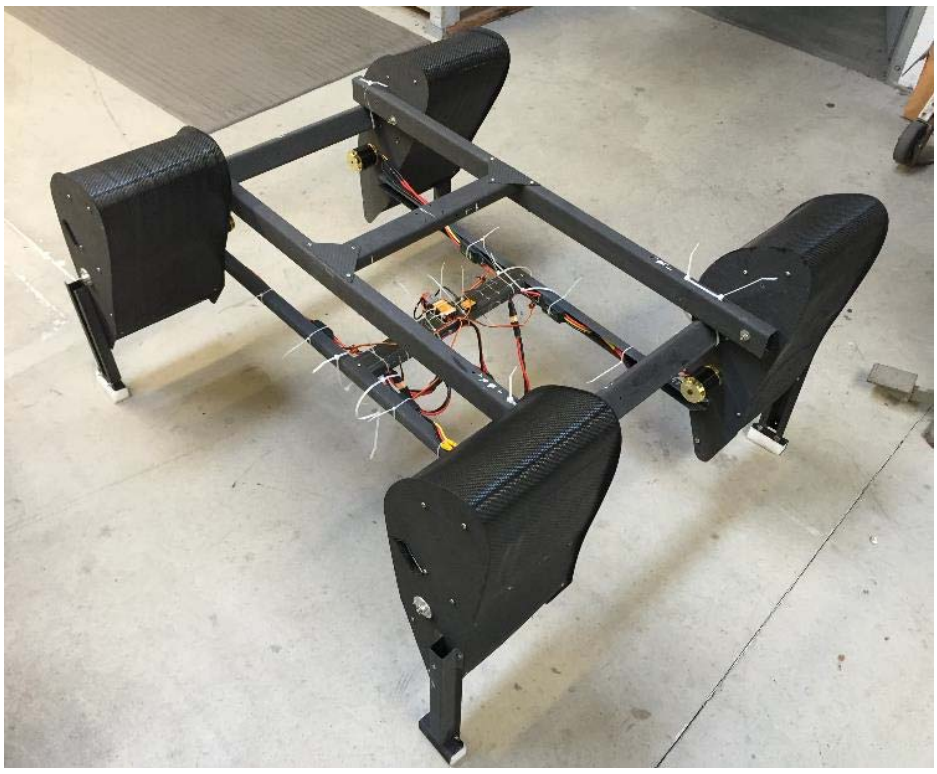

Figure 32. Fifth-generation, Mark IV.

Figure 33. Fifth-generation, Mark IV intended forward flight orientation.

Table 2. Mark IV vehicle material weight distribution.

	Mass, kg (lbs)	Percentage of Vehicle Mass
Airfoil	2.06 (4.54)	21.2%
Motor	1.82 (4.01)	18.7%
Wires, Fasteners, Frame	1.70 (3.75)	17.5%
Battery	1.63 (3.59)	16.8%
Endplate	1.24 (2.73)	12.7%
CFF	0.78 (1.72)	8.0%
ESC (motor controllers)	0.42 (0.93)	4.3%
Flight Controller	0.08 (0.18)	0.82%
Total	9.73 (21.5)	100%

III. FABRICATION

Wing and vehicle fabrication brought about several challenges. First, the wing needed to be built light enough for feasible flight. Second, the wing needed to be rigid enough to retain structural integrity under aerodynamic loads and pressure variations over the wing. Lastly, aircraft assembly needed to be designed in a way that enabled easy assembly, disassembly, maintenance, and modification.

A. AIRCRAFT MATERIAL SELECTION

Carbon fiber was used extensively throughout the vehicle due to its structural rigidity and lightweight characteristics. Pre-impregnated (prepreg) carbon fiber fabric from FibreGlast Inc. was used for the airfoil construction. This material was suitable due to its low cure temperature and flexible weave. Additionally, DragonPlate carbon fiber beams were used for the wing spars due to their high strength to weight ratio.

B. WING MOLD MANUFACTURING

Wing molds were made using additive manufacturing, also known as 3D printing. The goal of this process was to develop a less labor intense method of carbon part development than what was previously used. In the past, carbon layups were made using routed plywood mounted in a metal form. Figure 34 shows one such mold.

Figure 34. A former wood routed mold used for carbon fiber layup.

The idea behind additive manufacturing for mold generation is that in order to make a new design all that is needed is to draw the part using solid modelling and then send it to be 3D printed. The printer does the work and can be left unattended. For this manufacturing process, wing molds were printed on a Glacier Summit InDimension3 printer. Figure 35 shows the printed front and aft section wing molds. The front portion took 110 hours of print time and the aft section took 24 hours of print time. The front mold was printed in 2.54 cm (1 in) thick sections and the aft in 5.08 cm (2 in) thick sections.

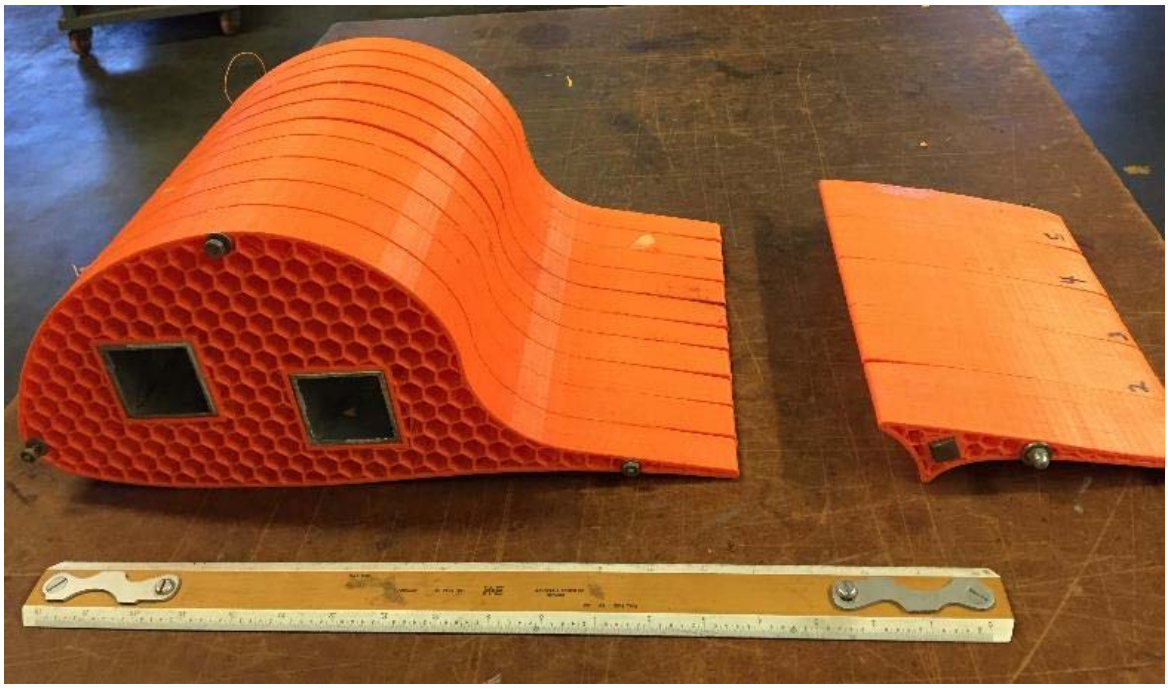

Figure 35. 3D printed wing molds.

1. Mold Filament Selection

The biggest requirement for the mold filament was that it had a high glass transition temperature. The filament needed to be able to withstand oven temperatures and pressures from the vacuum bagging. Three filaments were tested, but ultimately the filament chosen was Acrylonitrile Butadiene Styrene (ABS) made by Inland. Other filaments considered were Polylactic Acid (PLA) and Polycarbonate.

The required temperatures for the prepreg carbon to cure were provided in a data sheet by the manufacturer FibreGlast, given in [18]. Further testing was conducted on the prepreg carbon to determine if the carbon could be cured at lower temperatures than what was indicated. Figure 36 shows successful and unsuccessful prepreg carbon cure temps along with glass transition temperatures of the plastic mold filaments. PLA plastic has the lowest glass transition temperature of the three filaments and fell below any of the successful prepreg carbon cure temperatures. Polycarbonate was originally selected due to its ability to withstand high temperatures, but suffered from poor bed adhesion and significant warping while printing. ABS's glass transition temperature came in the middle, and could withstand lower bake temperatures. Simultaneously, the prepreg carbon could cure at temperatures as low as 80 ºC (175 ºF) provided it was baked for 12 hours.

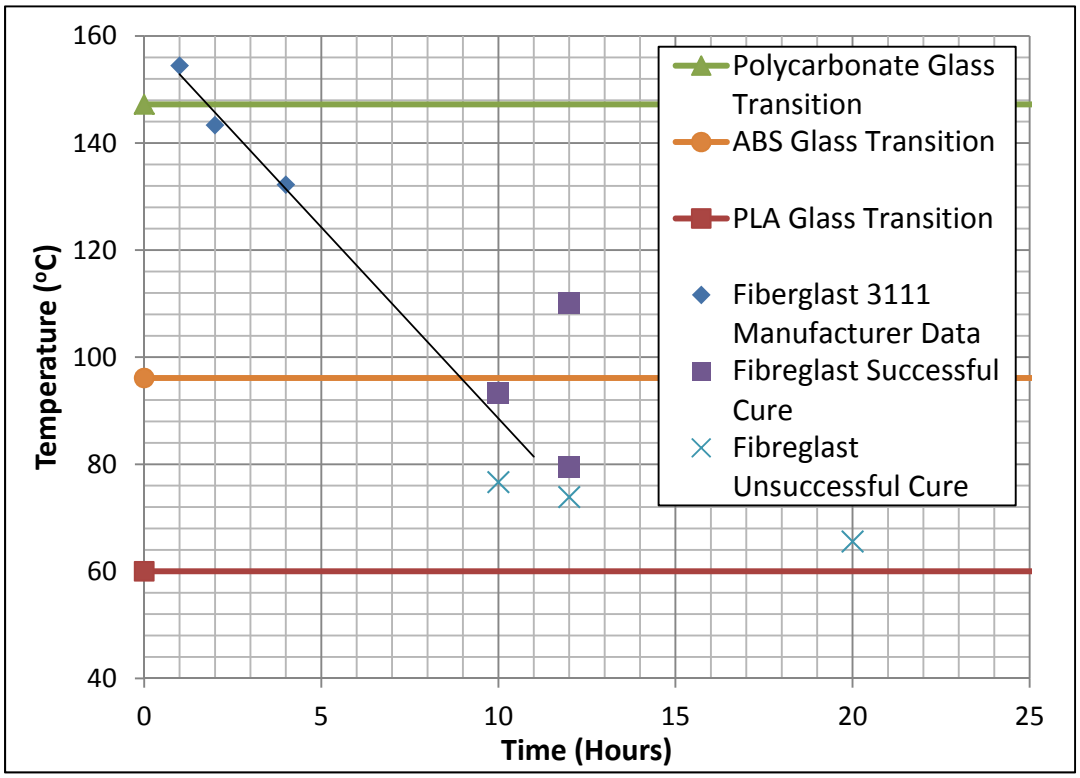

Figure 36. Carbon fiber cure temperatures and filament glass transition temperatures.

2. Print Quality Techniques

Glacier Summit's InDimension3 printer was used along with Repieter 3D printer software, which used Slic3r's gcode-generation engine. Several techniques and modifications were made in order to optimize print quality. Simplify3D [19] is an excellent guide for print quality troubleshooting.

a. Software Settings

Repieter's software settings are shown in Appendix D. They were baselined from settings optimum for printing PLA, which is generally considered very easy to print.

(1) Infill

Hexagonal infill, also known as honeycomb, was used due to its low density nature and structural integrity. Several factors were balanced in choosing infill density. First, lower infill densities printed more quickly, however, lower infill densities also lead to lower structural integrity—which needed be high enough to handle the vacuum bagging pressures at the elevated oven temperatures. Second, higher infill densities lead to more warping. Figure 37 shows 10%, 15% and 20% infill percentages in a honeycomb style. 15% infill was used for the aft section mold and 12% infill for the front section mold.

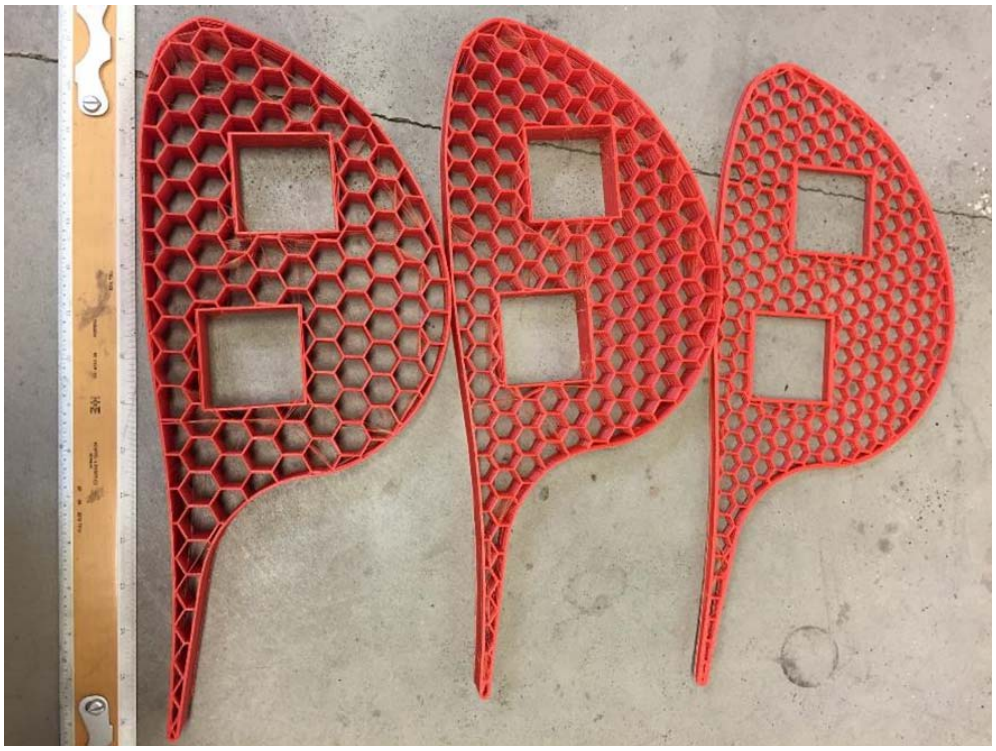

Figure 37. 10%, 15%, and 20% octagonal infill.

(2) Temperatures

Temperature greatly affected the print quality. Too low a print temperature resulted in layer delamination. However, due to the filament's thermal expansion coefficient, greater print temperatures resulted in more warping of the printed part. For the best print, the lowest temperature that resulted in good layer lamination was used. Print temperatures used were 235 ºC (455 ºF) for the first layer and 220 ºC (428 ºF) for the following layers.

(3) Extrusion

Extrusion rate affected layer lamination. Too low an extrusion rate resulted in poor layer lamination and an increased warping tendency due to the melted filament being stretched as it was laid down. Too high an extrusion rate resulted in the print-head nozzle jamming on the printed part. An extrusion multiplier between 1.05 and 1.1 resulted in best print quality. Figure 38 shows a part with over-extrusion that was corrected halfway through the printing.

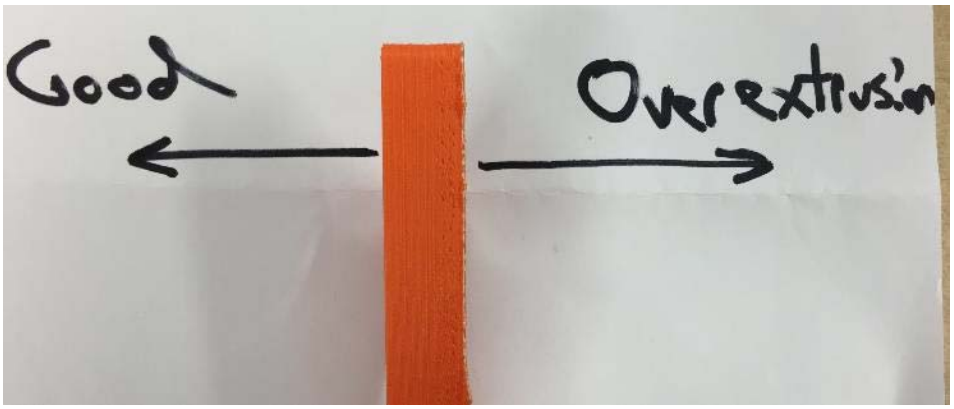

Figure 38. Correct and over-extruded extrusion rates.

(4) Speed

Lower print temperatures required slower print speeds due to the increased filament viscosity. Slower print speeds also increased layer adhesion, but needed be kept high enough so as to not cause local melting of the print part.

b. Bed Adhesion

Bed adhesion was one of the most difficult parts of printing ABS. Due to the print filament's coefficient of thermal expansion, large forces were exerted on the print bed when airing. This required the print to have a strong adhesion to the bed and the bed to have the rigidity necessary to resist warping. Printing with ABS juice on a sandblasted glass print bed, described in the following, accomplished both requirements.

(1) ABS Juice

ABS juice was made using ABS filament and Acetone. The filament was snipped into small pieces and placed in a mason jar, then filled with Acetone and given 24 hours to dissolve. Optimum proportions are given by [20], which recommended the juice be thinner than milk and thicker than water. Figure 39 shows the components of the ABS juice.

Figure 39. ABS juice components.

(2) Sand-blasted Glass Print Bed

A glass sheet was sandblasted and clamped to the print bed as shown in Figure 40. This was required because the prior print surface peeled off of the reinforcing metal plate heater when the front section of the airfoil mold was printed. Holding clips for the glass sheet were arranged so the print-head nozzle would not collide during print moves.

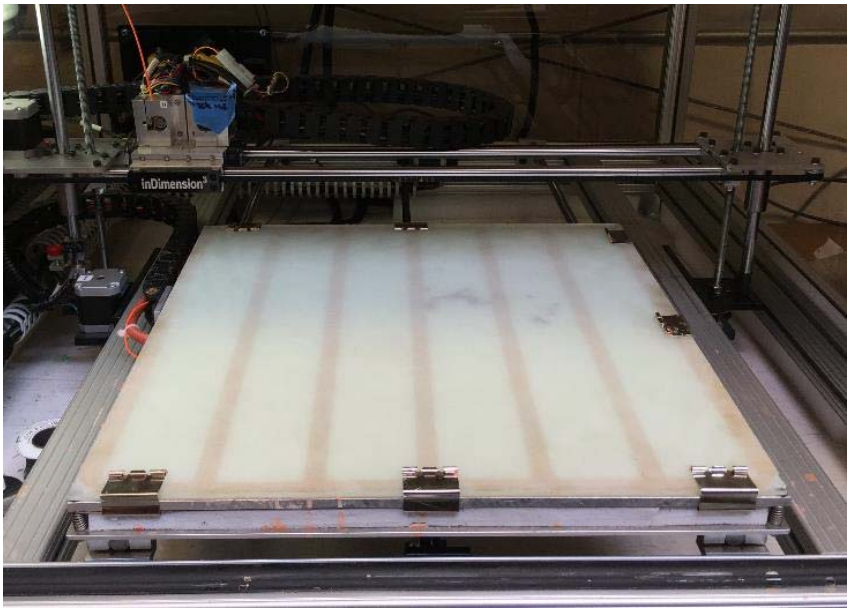

Figure 40. Sand-blasted glass print bed with clips.

c. Printer Modifications

Several modifications were made to the printer setup in order to improve print quality. First, the printer was insulated by covering ventilation openings with plastic foam. This increased the print atmosphere temperature which slowed the extruded material's cooling rate and decreased part warping. Second, the support material nozzle cooling fan was reversed in order to decrease the amount of air blown down on the part and thus slow the cooling rate. Third, the filament was run through a tensioner to prevent it from jumping off the spool in large print-head movements. The tensioner was a piece of plastic foam mounted above the printer that the filament ran through.

3. Mold Assembly

Printed molds were assembled using all-thread and rectangular metal beams. The assembled molds were heated in the oven at 82 ºC (180 ºF) with the all-thread nuts loosened to prevent the mold from cracking due to the thermal coefficient of expansion mismatch between the ABS plastic and the steel all-thread. ABS expands more than steel when heated. Once the molds were at oven temperature the all-thread nuts were gradually

tightened until any gaps between mold parts were closed. This process took about 20 hours of oven bake-time and aligned any partially warped parts for better mold quality.

C. CARBON FIBER WING LAYUP

The wing airfoil parts were manufactured using a prepreg composite layup process. Five layers of carbon were used for the aft section and three layers for the front section with two additional layers in the back near the CFF. Parts were bagged and vacuumed while being baked in a traditional kitchen style oven.

1. Bagging

FibreGlast clear bagging material was cut and made into the bags to be vacuumed down over the layup. The front and aft sections of the airfoils were laid up separately and also baked separately. In order to ensure the bag vacuumed down correctly in the oven, a vacuum pump was attached while the layup was still on the original layup table. Figure 41 shows the setup.

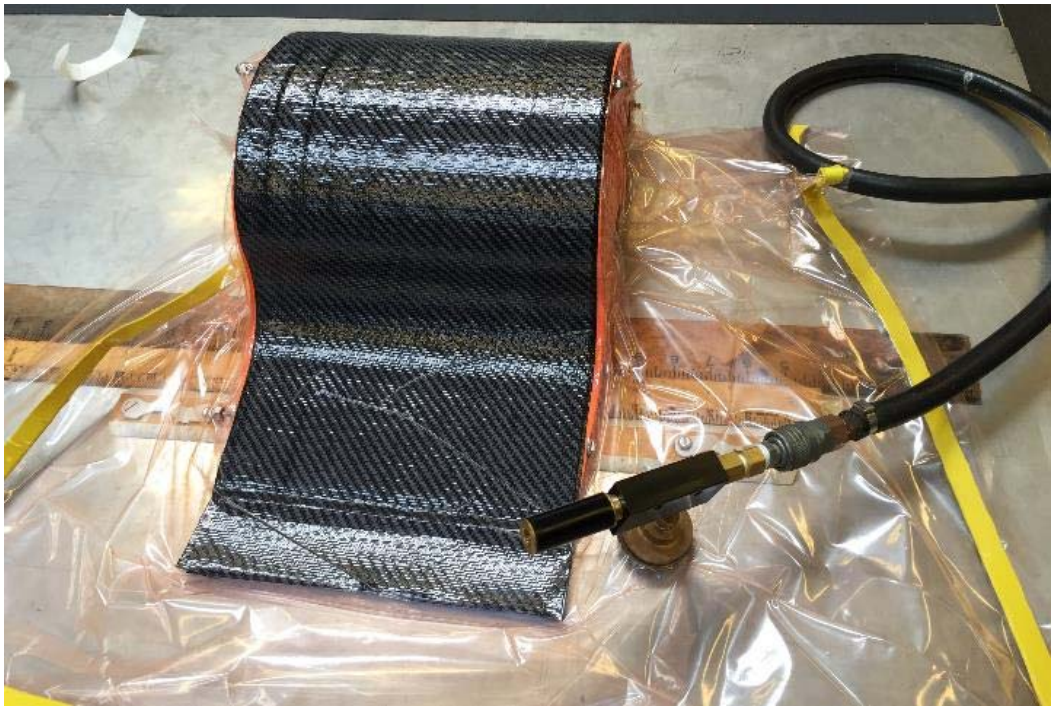

Figure 41. Bagging and vacuum pump usage.

2. Releasing Agent

Coconut oil was used as the releasing agent. Molykote® was also tested for comparison. Molykote® inhibited the prepreg carbon from fully curing at the bake temperatures of 82 ºC (180 ºF). Additionally, the coconut oil left a nicer surface finish as Figure 42 shows, and was solid at room temperature—making application easy and clean.

Figure 42. Molycote and coconut oil releasing agent comparison.

The ABS mold had a tendency to stick to the prepreg carbon—even with the releasing agent—and tear out chunks of the mold when taken apart. Figure 43 shows a case of this. The remedy was to coat a sheet of the clear bagging material on both sides with coconut oil and place it between the mold and carbon.

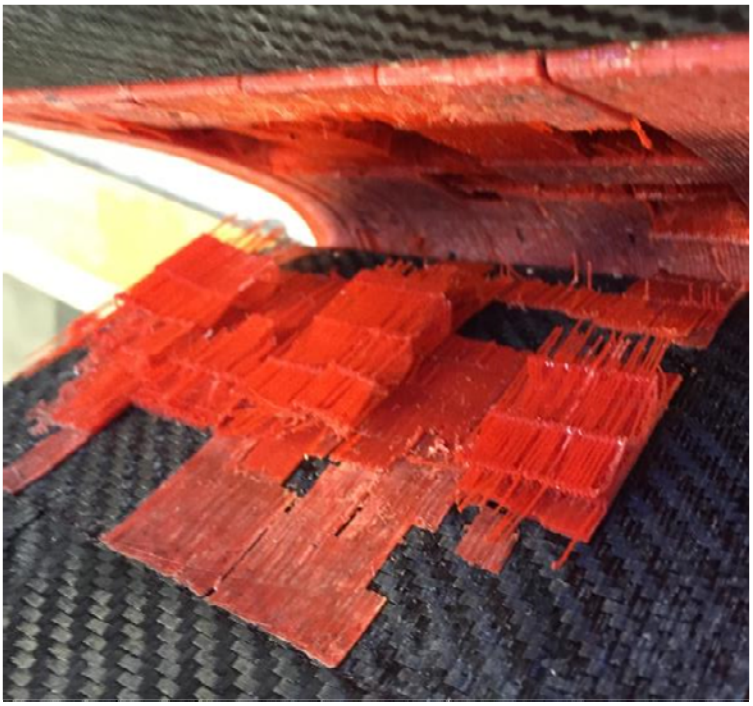

Figure 43. Mold breakdown.

3. Baking

Layups were baked for 12 hours at 82 ºC (180 ºF) with a vacuum pump continuously running. Caution had to be taken while using ABS in the oven. While the bake temperatures were not high enough to melt the ABS, the heater filament, when on, was much higher than the ABS could withstand. Two things were done to avoid mold collapse. First, the oven was preheated to 85 ºC (185 ºF), and then decreased to 82 ºC (180 ºF) directly before putting the layup in the oven. This helped prevent the heater coil from turning on to high intensity when opened for layup placement. Second, the layup was placed on a piece of plywood, which was placed on a piece of thick sheet metal directly over the heater coil. The sheet metal prevented the heater coil from burning any of the layup, and the plywood acted as insulation to prevent the radiant heating of the heater coil from locally melting the mold. Figure 44 shows a mold with local structure collapse due to overheating from radiant heat off the heater coil.

Figure 44. Local mold collapse due to radiant overheating.

4. Trimming Airfoil

The airfoils were made 24 cm (9.5 in) wide and cut to 22.9 cm (9 in) to ensure straight sides and consistent edge thicknesses. A DeWalt tile saw, Figure 45 was used on the aft sections and a carbide bladed band saw, Figure 46, was used to cut the front section since it was too large to fit through the tile saw. The band saw was hooked up to two industrial vacuum cleaners in order to minimize carbon particles released into the air. Alternatively, the tile saw used a built-in water system to stop carbon dust release.

Figure 45. DeWalt tile saw used for trimming aft wing airfoils.

Figure 46. Carbide grit band saw used for trimming fore wing airfoils.

D. WING ASSEMBLY

Wing assemblies were designed and built with two considerations. First, they needed to be very rigid in order to hold the CFFs in position and act as load bearing components of the frame, and second, they needed to be simple to assemble and disassemble. Brackets were epoxied onto the inner surface of the airfoils. Clothespins provided sufficient clamping force to hold the brackets in place while curing. Figure 47 shows brackets in place ready to be glued and Figure 48 shows the brackets glued in place with clip nuts attached. These clip nuts enabled the end-plates to be attached without the need to access the inside. Screws were used instead of bolts to enable self-alignment upon insertion.

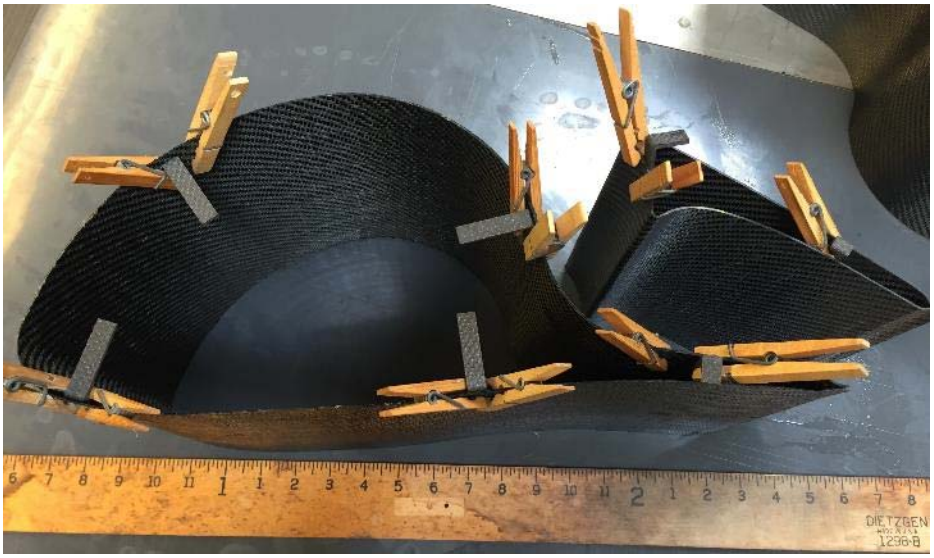

Figure 47. Wing with brackets at final spacing.

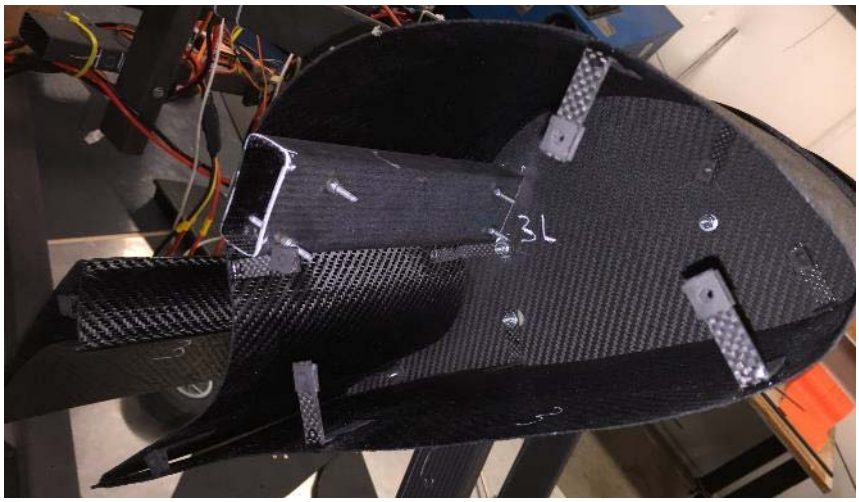

Figure 48. Wing with brackets glued and clip nuts attached.

End-plates were cut commercially by Advanced Laser & Waterjet Cutting using the profiles shown in Figure 49. Advanced Laser & Waterjet Cutting used a CNC laser cutter in an inert atmosphere to cut the end-plates. The inert atmosphere prevented the carbon and resin from igniting under the laser beam.

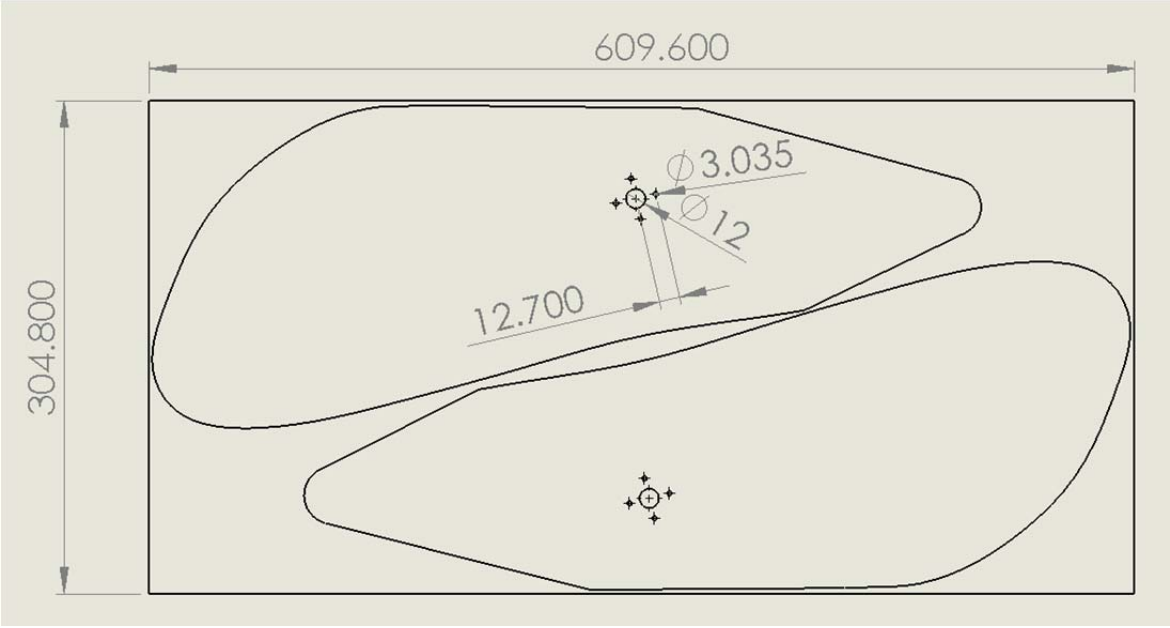

Figure 49. End-plate design used by Advanced Laser & Waterjet Cutting for the end-plates. Dimensions are in mm.

The fan was aligned by wrapping felt around it while assembling the wing. Figure 50 illustrates. The felt ensured enough spacing around the fan so it would not rub on the casing, approximately 0.3 cm (1/8th in), but not too large a gap as to make assembly impossible or significantly degrade performance by blade tip leakage. Figure 51 shows a completely assembled wing. The design is modular and can be easily adapted to vehicle changes.

Figure 50. Felt used to properly align and space CFFs.

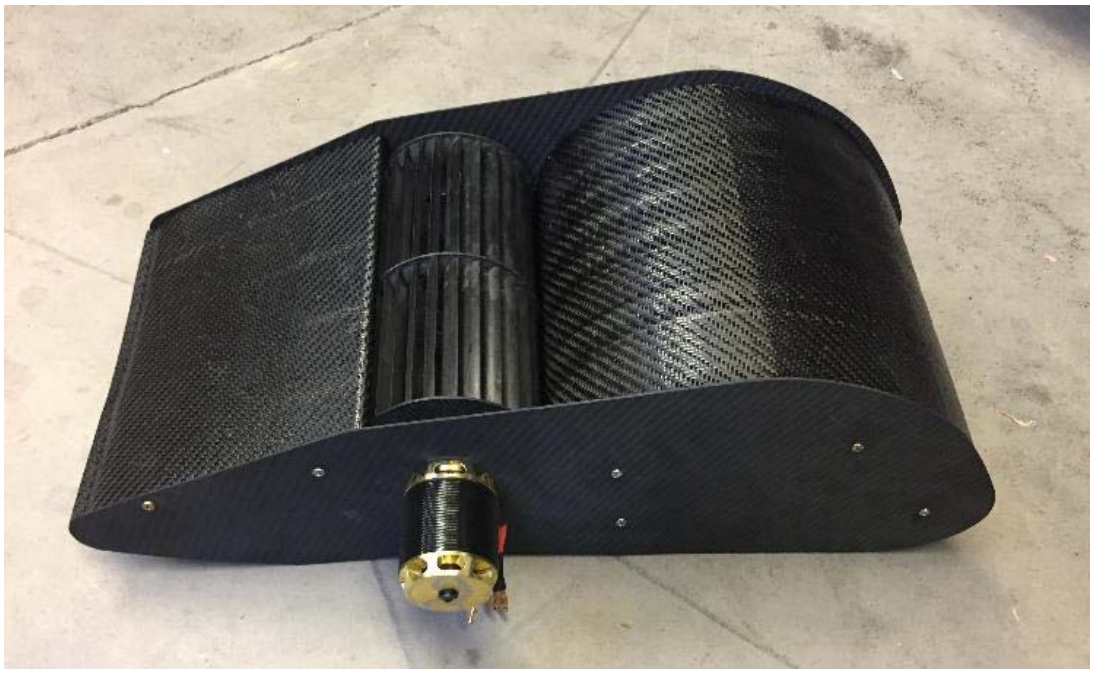

Figure 51. Fully assembled wing.

E. FRAME ASSEMBLY

The main goal in assembling the aircraft was to have a rigid frame that could withstand hard impacts and crashes but was also light-weight. Beams for the frame assembly were selected based on experimental measurements of weight and torsional rigidity. The airfoil assemblies were integrated thoroughly into the frame as stiffeners because of their high rigidity. This allowed a reduced usage of gusset plates and an overall decrease in vehicle weight.

1. Beam Selection

Vehicle frame material selection was based on experimental data, and the intended purpose of the particular frame member. Several beam types with varying cross-sections, Figure 52, were weighed for specific mass-per-length and tested for torsional rigidity.

Figure 52. Potential frame member cross-sections.

Torsional rigidity was calculated using Equation (8) where G is the shear modulus, I is the polar moment of inertia, T is the applied torque, L is the length, and Θ is the angular twist.

$$GI = \frac{TL}{\theta} \tag{8}$$

G*I was calculated because both quantities correspond to greater stiffness at larger values. Figure 53 shows the experimental setup. In the bottom right corner is a support that prevents the beam from bending and only lets it twist torsionally. Table 3 shows the rigidity and specific mass properties.

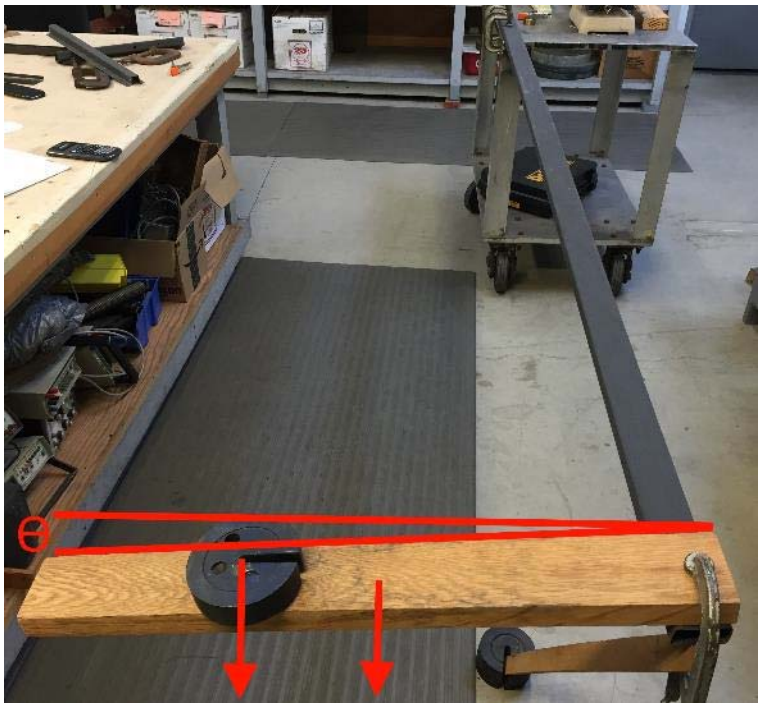

Figure 53. Torsional rigidity measurement experimental setup.

Table 3. Specific mass-per-length and torsional rigidity.

	Mass-per-length, kg/m (lbs/ft)	**Torsional Rigidity: G*I, N m^2/rad (lbs ft^2/rad)**
Rectangular	0.20 (0.13)	193 (467)
Top-hat Side Flange Connection	0.11 (0.074)	0.62 (1.5)
Top-hat Middle Connection	0.11 (0.074)	0.015 (0.036)
Shallow Channel	0.10 (0.067)	0.52 (1.3)
Deep Channel	0.10 (0.067)	0.34 (0.82)

The rectangular cross-section was by far the most torsionally stiff and also the heaviest. This beam was used to make a stiff box structure that connected the parallel wing assemblies and also formed a front to back dual spine to connect the two pairs of wing assemblies. Deep channel beams were used for the lower beams to hold the

electronics and prevent wing rotation. They were used because they were easily connected to the controller supporting beam, and additionally were the lightest option and not in a position subject to much torsional stress.

2. Airfoil-Frame Integration

Parallel airfoil assemblies were joined with rectangular cross-section beams as shown in Figure 54. The beams were bolted using locknuts into a portion of the airfoil that was five carbon layers thick.

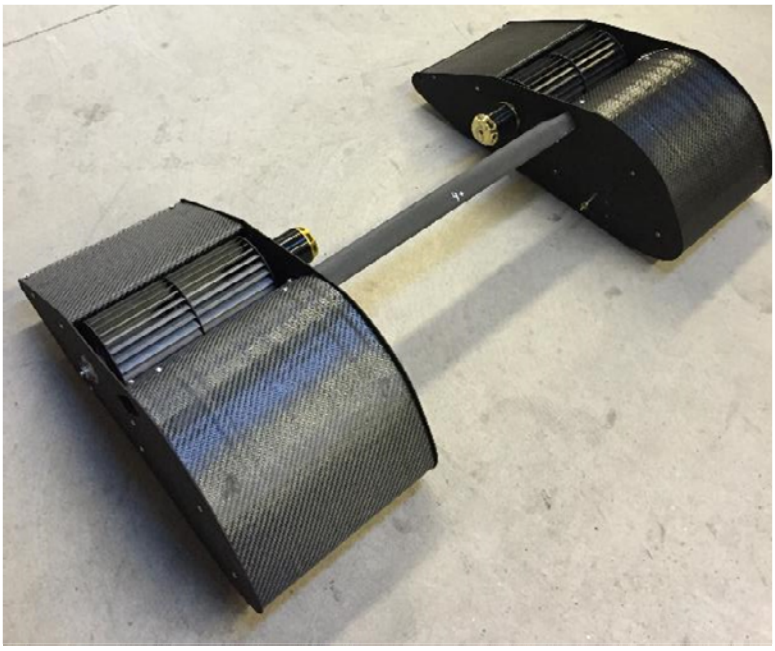

Figure 54. Paired airfoil assemblies on a common spar.

The connection between the airfoils and connecting beam locked the endplates and beam together as if there was a gusset plate between the two. This allowed structural members to be connected directly into the endplates as shown in Figure 55.

Figure 55. Frame members hooked directly to the endplates.

3. Landing Gear

Landing gear was used to cushion landing and hold the entire aircraft up to keep the aft section of the wing assemblies off the ground. When too close to the ground, the wings had a tendency to push the aircraft backward due to their outlet jets being angled forward. The first landing gear used was a set of wheels that each weighed 0.25 kg. These proved unnecessarily heavy and were exchanged for curved carbon struts similar to what was used in [5]. This landing gear setup was flexible and supported the aircraft while providing a cushion. However, during testing it was too fragile to handle rough landings and was exchanged for four vertical struts with cushioned foam blocks, as shown in Figure 56.

Figure 56. A vertical landing strut.

IV. VEHICLE TESTING

A. VERTICAL HOVER

1. Tethered Indoor Flight

Initial flight testing was conducted using a tether to prevent the aircraft from crashing. The tether was similar to a dog run and allowed vehicle operation within a large area. Figure 57 shows a successful tethered flight.

Figure 57. Tethered vertical hover.

2. Untethered Indoor Flight

Once the gains on the flight controller were correctly set, the aircraft was able to hover quite stably. Figure 58 shows an untethered indoor flight. Appendix E contains the Naza-M flight controller settings used.

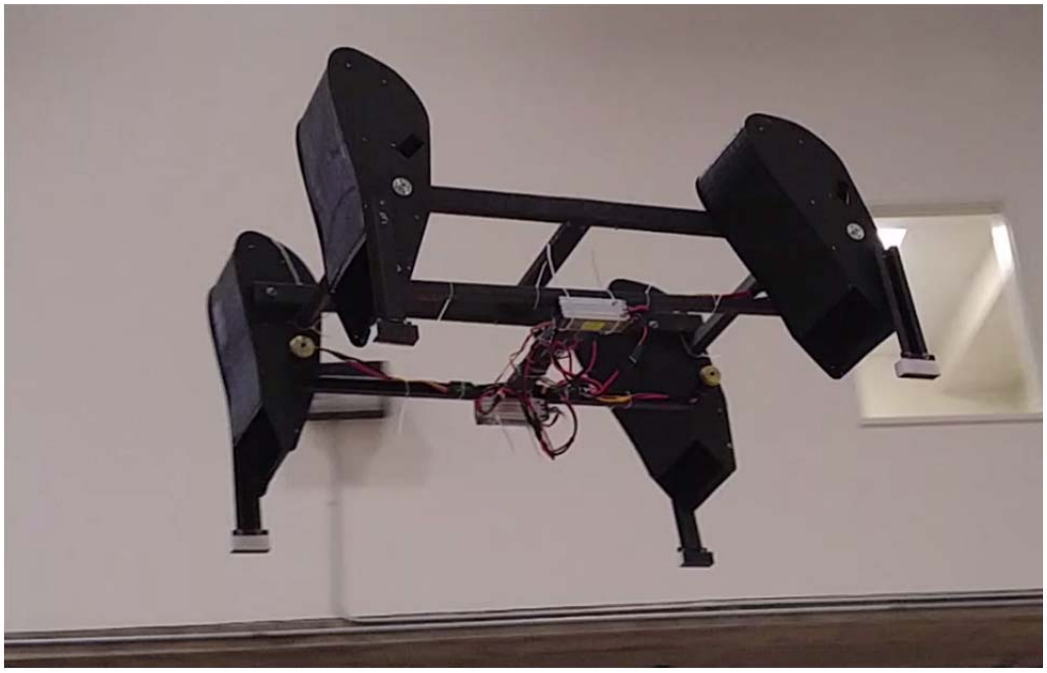

Figure 58. Untethered vertical hover.

Flight testing found that the electrical system overheated after about 10 seconds of flight. Electrical testing was conducted and found that with a 25 V supply voltage, each motor used 160 A. Closer investigation was made into what the optimum motor would be for the aircraft. Appendix F tabulates a large quantity of Scorpion motors based on their ratings. The important qualities the motors must have are a high maximum continuous power and a low Kv rating. Kv rating specifies how many RPM a motor turns per volt applied. Low Kv ratings indicate high torque motors and high Kv ratings indicate high speed motors. The CFFs spin at relatively low RPMs in comparison to the speeds most Scorpion motors are intended to operate (~7,000 RPM versus ~13,000 RPM). When the motors are operated at RPMs lower than what they are designed for they draw more current, which can overload the electrical system and cause it to overheat.

V. CONCLUSIONS

A wing embedded, cross-flow fan powered aircraft capable of vertical takeoff and landing was designed based on the Gottingen 570 and characterized over a TSR range of zero (hover) to infinity (glide) using Ansys CFX solver. Two-dimensional simulation predicted a hover angle of 36º with 56% of the lift coming from the airfoil and 44% coming from the CFF. 3D simulation predicted a slightly larger hover AOA of 56º while actual flight testing found the wing hovered at 60º. This meant that the wing needed less than a full 90º rotation to go from hover to conventional flight.

Fabrication of the airfoils used prepreg carbon layups on 3D printed molds that were capable of withstanding elevated oven temperatures and vacuum pump pressures. Printer filament for the printed molds was ABS and was chosen based on its high glass transition temperature and relative ease of printing.

Assembled wings measured 0.2286 m (9 in) in width and 0.5 m (19.7 in) in chord length and were arranged in a quad configuration with all wings facing the same direction, which was counter to previous designs that used symmetry to increase stability, but favored forward flight. Overall aircraft dimensions were 1.2 m (4 ft) long, 0.91 m (3 ft) wide, and 0.61 m (2 ft) high for a total weight of 10 kg (21 lbs). Controlled untethered flight was successful and stable.

THIS PAGE INTENTIONALLY LEFT BLANK

VI. RECOMMENDATIONS AND FUTURE WORK

Future work on wing-embedded, cross-flow-fan, vertical takeoff and landing air vehicles could include improvements to the wingtip design and electrical power system, and decreasing the aircraft weight. Potential vehicle design changes include actuating the wings to shift from hover to conventional flight. On wingtip design, the wings could be extended in order to generate a more 2D flow over the wings, or alternatively rounded wing tips could be added to generate additional lift off the smooth flow over contoured tips compared to the present presumably separated flow. The electrical power system could be improved by replacing the present motors with lower speed higher torque motors or by running the motors through a gearbox or belt system to allow the motors to run at higher speeds than the CFFs. Additionally, in order to prevent electrical current overload, the operating voltage could be increased to 50 V instead of the present operating voltage of 25 V. In order to decrease aircraft weight, the aft airfoil layup material could be reduced from five layers of carbon to three or fewer layers, and the front could be made with two layers all around and four in the CFF housing section. Additionally, the end plates could be made out of thinner carbon fiber sheets.

THIS PAGE INTENTIONALLY LEFT BLANK

APPENDIX A. MATLAB SCRIPT FOR IMPORTING WING GEOMETRY

```
clear,close all,clc
%  ------------------------------------------------------------------------
--
% USER INPUT
x_shift = 0;     % m
y_shift = -0.01;      % m
scale = 0.5;      % 0-1
alpha_deg = 0;    % degrees
offset_angle = 0; % degrees
airfoil = 'goe570.dat'
S                          =                          urlread(['http://m-
selig.ae.illinois.edu/ads/coord/',num2str(airfoil)]);    %    reads    in
coordinates from a webpage
temp1=strfind(S,'0.0');
temp2=strfind(S,'1.0');
temp3=min([temp1(1) temp2(1)]);
S = S(temp3:end);
%  ------------------------------------------------------------------------
--

S = str2num(S);
S = [S zeros(length(S),1)];
mid = find(S(:,1)==0);
mid = mid(2);
S = [S(1:mid-2,:); flipud(S(mid:end,:))];

% Rotor Constants
s_thick  = 0.001;  %Slice thickness in meters
vawt_radius  = 0.61;  %VAWT Radius

% Rotation Input
alpha=alpha_deg*pi/180.0;
x = S(:,1);
y = S(:,2);
plot(x,y,'r.')
grid on

% Scale
x = x*scale;
y = y*scale;

% Translate
c = x(mid);
DELX = 0.65*c+x_shift;
DELY = 3*0.61*(-0.02)+y_shift;
for i=1:length(S);
    X(i) = x(i)-DELX;
    Y(i) = y(i)+DELY;
end
```

```
%Rotate
for i=1:length(S);
    XX(i) = X(i)*cos(alpha)+Y(i)*sin(alpha);
    YY(i) = -1*(X(i)*sin(alpha)-Y(i)*cos(alpha));
end

%Plot Shifted Wing
hold on
plot(XX,YY,'b')

%Plot CFF Circle
plot([-.05:.01:.05],[sqrt(.05^2-[-.05:.01:.05].^2)],'k');
plot([-.05:.01:.05],[-sqrt(.05^2-[-.05:.01:.05].^2)],'k');
%axis([-.4 1 -.4 1])

xyz=[XX;YY]';
xyz(:,3)=0;
xyz

% Close the curves
Grid.X = xyz(:,1);
Grid.Y = xyz(:,2);
Grid.Z = xyz(:,3);

% Start solidworks and close all open SolidWorks files
% interop services file
NET.addAssembly('C:\Program                              Files\SolidWorks
Corp\SolidWorks\SolidWorks.Interop.sldworks.dll');
% Create Solidworks app in
swApp = SolidWorks.Interop.sldworks.SldWorksClass;
swApp.CloseAllDocuments(true);

% Make application visible
if ~(swApp.Visible)
    swApp.Visible = true;
end

% Template with SI units is opened
Part  = swApp.OpenDoc6([pwd '\parts\Template2.SLDPRT'], 1, 0, [], 0,0);

%This allows geometries of less than 1mm
Part.SketchManager.AddToDB = true;
Part.SketchManager.DisplayWhenAdded = false;

%Draw Square
Part.Extension.SelectByID2('Front Plane','PLANE',0,0,0,false,0,[],0);
Part.SketchManager.InsertSketch(true);
Part.SketchManager.CreateCornerRectangle(-10, -5, 0, 5, 5, 0);
Part.SketchManager.InsertSketch(true);
Part.ShowNamedView2('Isometric', 7);

% Extrude Square
```

```
Part.FeatureManager.FeatureExtrusion2(true,false,false,0,0,s_thick,...

s_thick,false,false,false,false,0,0,false,false,false,false,true,...
    true,true,0,0,false);
Part.ClearSelection2(true);

% Base wing profile
Part.Extension.SelectByID2('Front Plane','PLANE',0,0,0,false,0,[],0);
Part.InsertCurveFileBegin;
for jj = 1:length(S);
    Part.InsertCurveFilePoint(Grid.X(jj),Grid.Y(jj),0);
end
Part.InsertCurveFileEnd();

%Converts Curve to Sketch
Part.Extension.SelectByID2('Front Plane','PLANE',0,0,0,false,0,[],0);
Part.SketchManager.InsertSketch(true);
Part.Extension.SelectByID2('Curve1','REFERENCECURVES',0,0,0,true,0,[],0
);
Part.SketchManager.SketchUseEdge2(false);

%Extrude Cut
Part.FeatureManager.FeatureCut3(true,false,true,1,0,s_thick,s_thick,fal
se,false,false,false,0,0,false,false,false,false,  false,  true,  true,
true, true, false, 0, 0, false);
Part.ClearSelection2(true);

% Revert to user interface and zoom to fit
Part.SketchManager.AddToDB = false;
Part.SketchManager.DisplayWhenAdded = true;

% Extrude Stock CFF Profile
Part.Extension.SelectByID2('Sketch5', 'SKETCH', 0, 0, 0, false, 0, [],
0);
Part.EditSketch;
Part.FeatureManager.FeatureExtrusion2(true, false, false, 0, 0, 0.001,
0.01,    false,    false,    false,    false,    1.74532925199433E-02,
1.74532925199433E-02, false, false, false, false, true, true, true, 0,
0, false);

% Save As,  close template, open saved part, front view
Part.SaveAs3(['F:\Fulton\Macro_codes\parts\',num2str(airfoil),'_',num2s
tr(alpha/pi*180),'deg_',num2str(scale*100),'scale.SLDPRT'], 0, 2);
swApp.CloseAllDocuments(true);
Part                              =                swApp.OpenDoc6([pwd
'\parts\',num2str(airfoil),'_',num2str(alpha/pi*180),'deg_',num2str(sca
le*100),'scale.SLDPRT'], 1, 0, [], 0,0);
Part.ClearSelection2(true);
Part = swApp.ActiveDoc
Part.ShowNamedView2 ('*Front', 1);

% Rotate CFF fan
Part.Extension.SelectByID2('Sketch5', 'SKETCH', 0, 0, 0, false, 0, [],
0);
```

```
Part.EditSketch;
Part.Extension.SketchBoxSelect(0.120443, 0.096628, 0.000000, -0.092529,
-0.093114, 0.000000);
Part.Extension.RotateOrCopy(false, 1, false, 0, 0, 0, 0, 0, 1, -
alpha+offset_angle*pi/180);
Part.EditRebuild3()

% Resave Part with CFF Rotation
Part.SaveAs3(['F:\Fulton\Macro_codes\parts\',num2str(airfoil),'_',num2s
tr(alpha/pi*180),'deg_',num2str(scale*100),'scale.SLDPRT'], 0, 2);
```

APPENDIX B. ANSYS BLOCK DIAGRAM

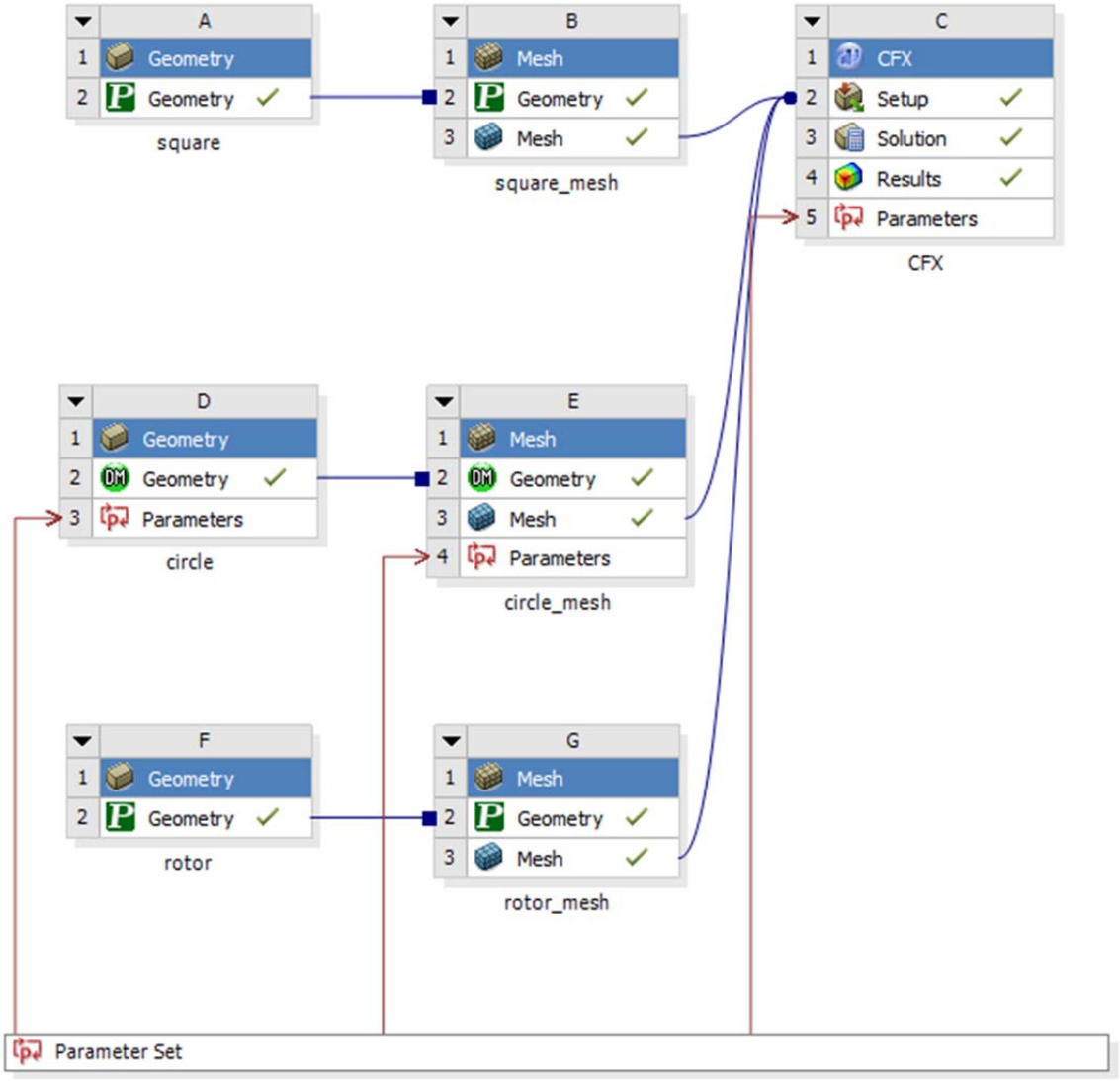

THIS PAGE INTENTIONALLY LEFT BLANK

APPENDIX C. ANSYS CFX VARIABLES, EXPRESSIONS AND USER-DEFINED CODE

Pre Expressions:

$$Airspeed = TSR * RPM * 0.1016\ [m]$$

Post Variables:

$$velDOTn = Velocity\ u * Normal\ X + Velocity\ v * Normal\ Y + Velocity\ w * Normal\ Z$$

Post Expressions:

$$AirfoilForceX = force\_x()@circle\ Default$$

$$AirfoilForceY = force\_y()@circle\ Default$$

$$JetVelocity = massFlowAve(Velocity)@jet$$

$$RotorThrustX = -sum((Velocity\ u - massFlowAve(Velocity\ u)@inlet\ ) * Density * velDOTn * Area)@jet$$

$$RotorThrustY = -sum(Velocity\ v * Density * velDOTn * Area)@jet$$

$$RotorTorque = torque\_z()@rotor\ Default$$

THIS PAGE INTENTIONALLY LEFT BLANK

APPENDIX D. REPIETER PRINT SETTINGS SCREEN SHOTS

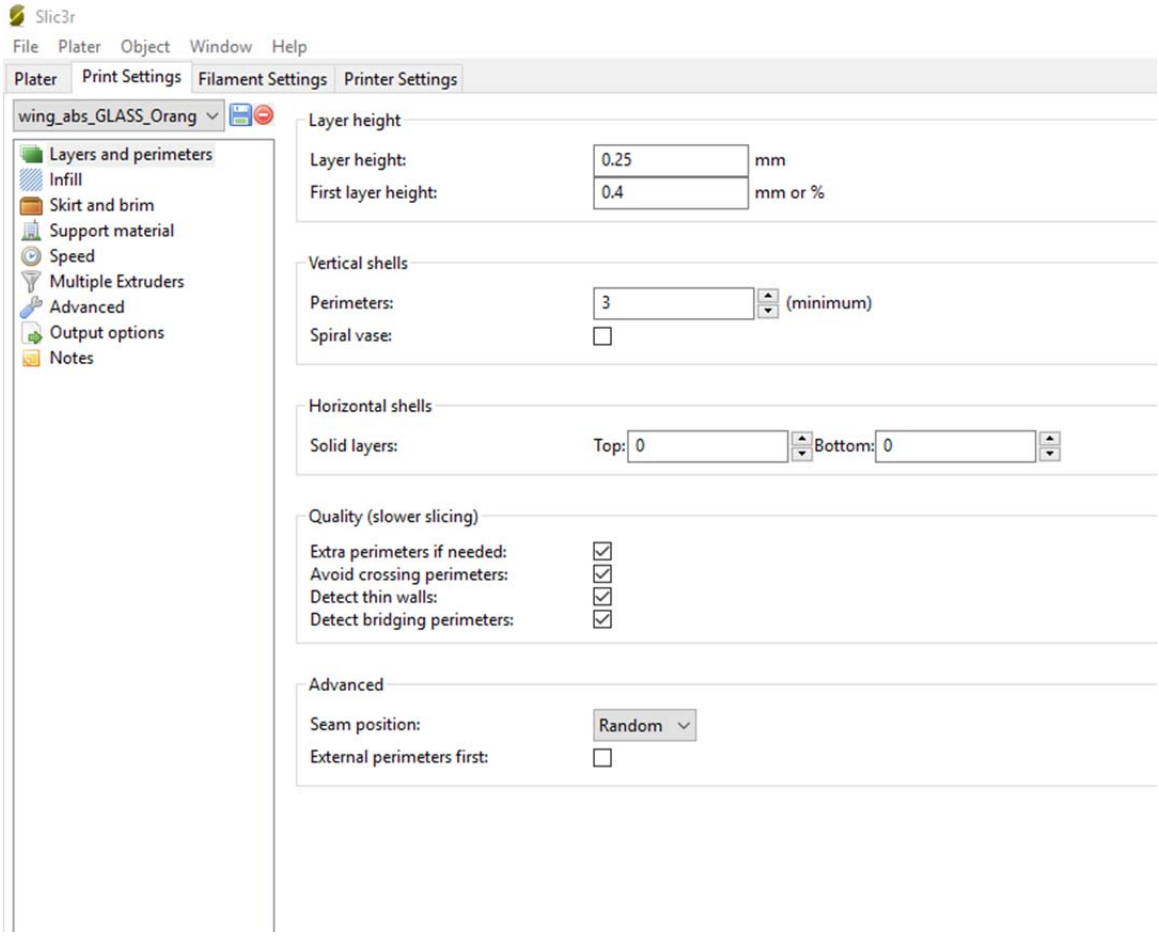

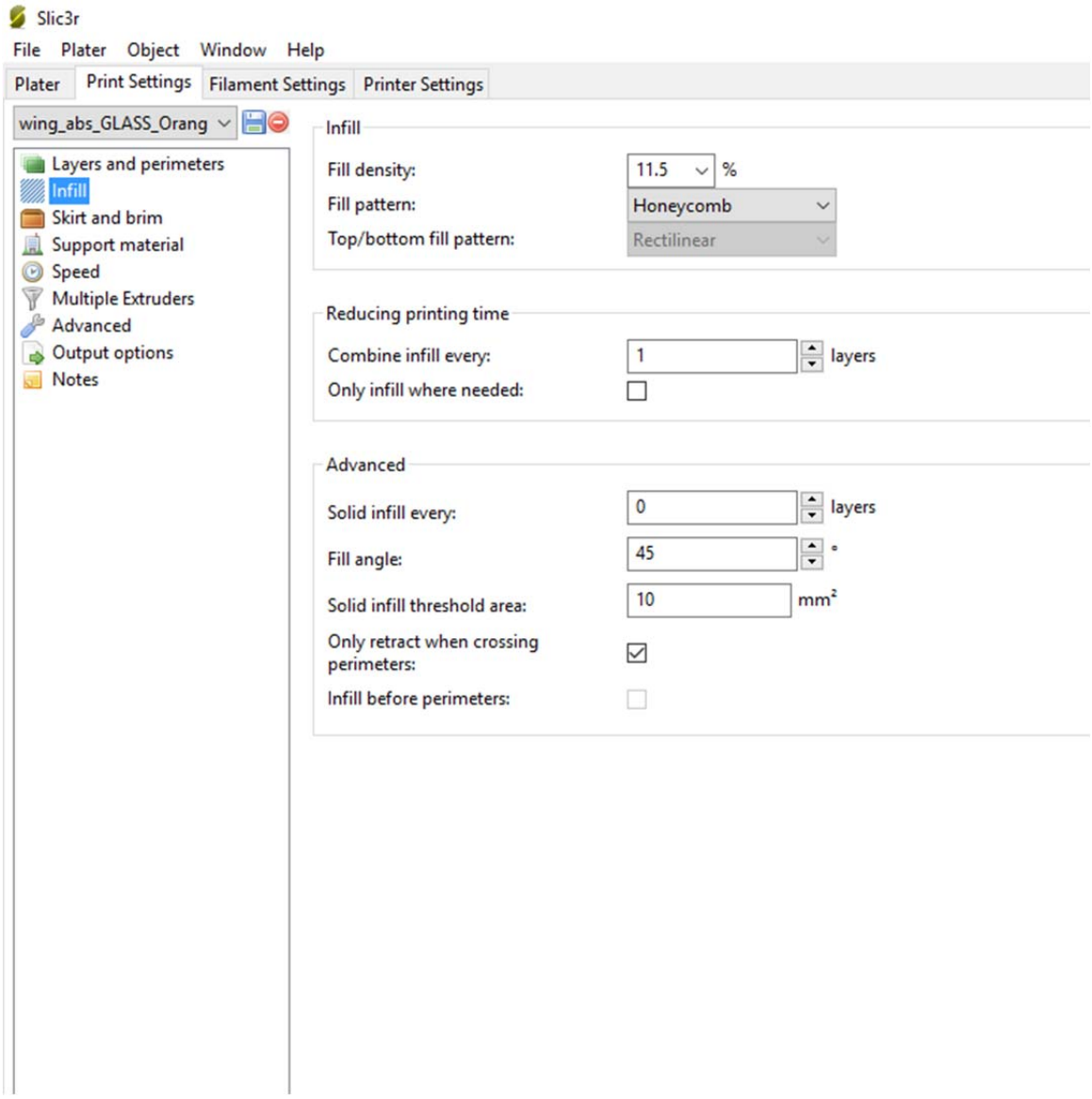
Slic3r
File Plater Object Window Help
Plater
Print Settings
Filament Settings
Printer Settings
wing_abs_GLASS_Orang
Layers and perimeters
Infill
Skirt and brim
Support material
Speed
Multiple Extruders
Advanced
Output options
Notes
Infill
Fill density:
11.5
%
Fill pattern:
Honeycomb
Top/bottom fill pattern:
Rectilinear
Reducing printing time
Combine infill every:
1
layers
Only infill where needed:
Advanced
Solid infill every:
0
layers
Fill angle:
45
°
Solid infill threshold area:
10
mm²
Only retract when crossing perimeters:
Infill before perimeters:

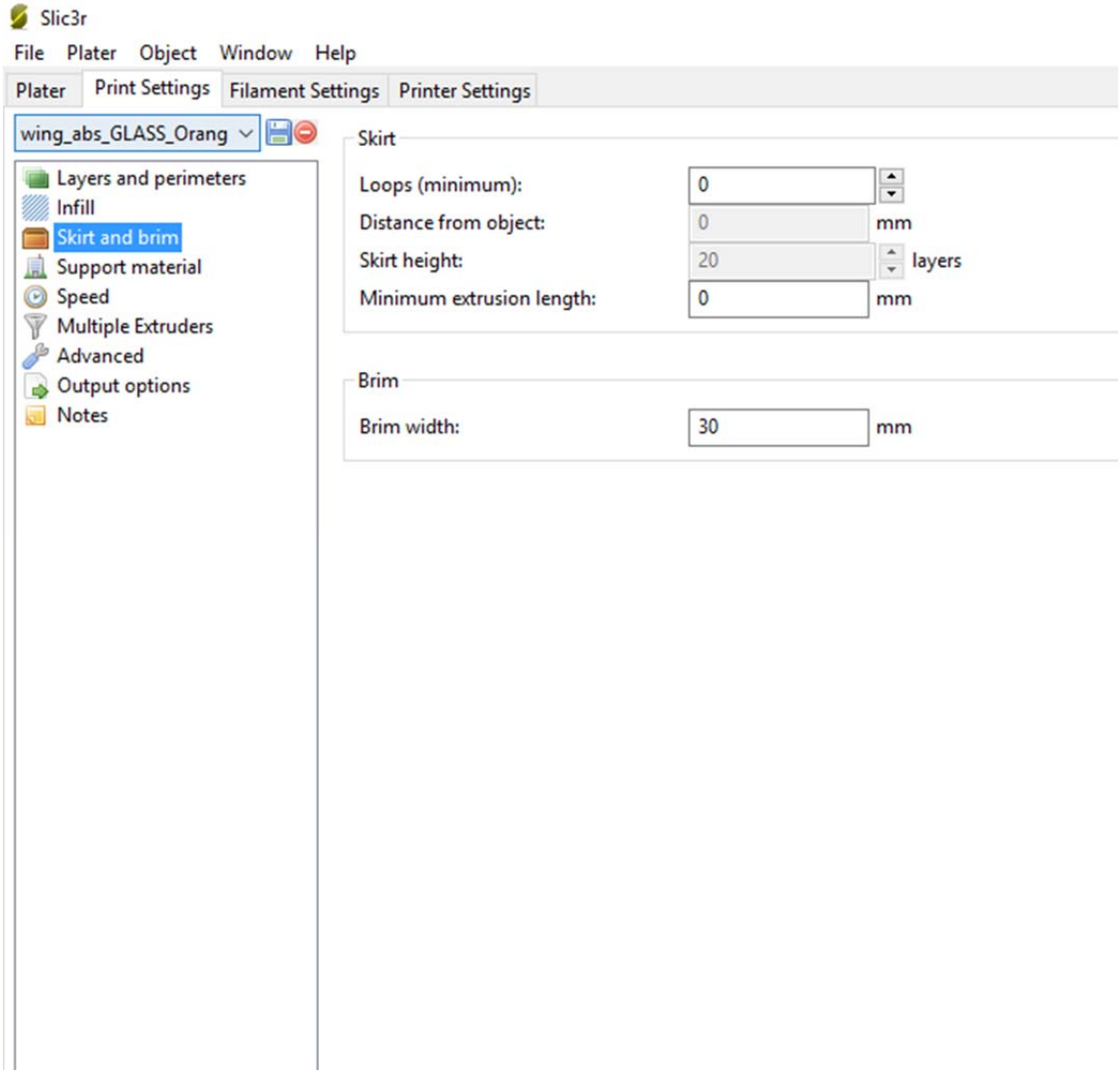
Slic3r
File Plater Object Window Help
Plater
Print Settings
Filament Settings
Printer Settings
wing_abs_GLASS_Orang
Layers and perimeters
Infill
Skirt and brim
Support material
Speed
Multiple Extruders
Advanced
Output options
Notes
Skirt
Loops (minimum):
0
Distance from object:
0
mm
Skirt height:
20
layers
Minimum extrusion length:
0
mm
Brim
Brim width:
30
mm

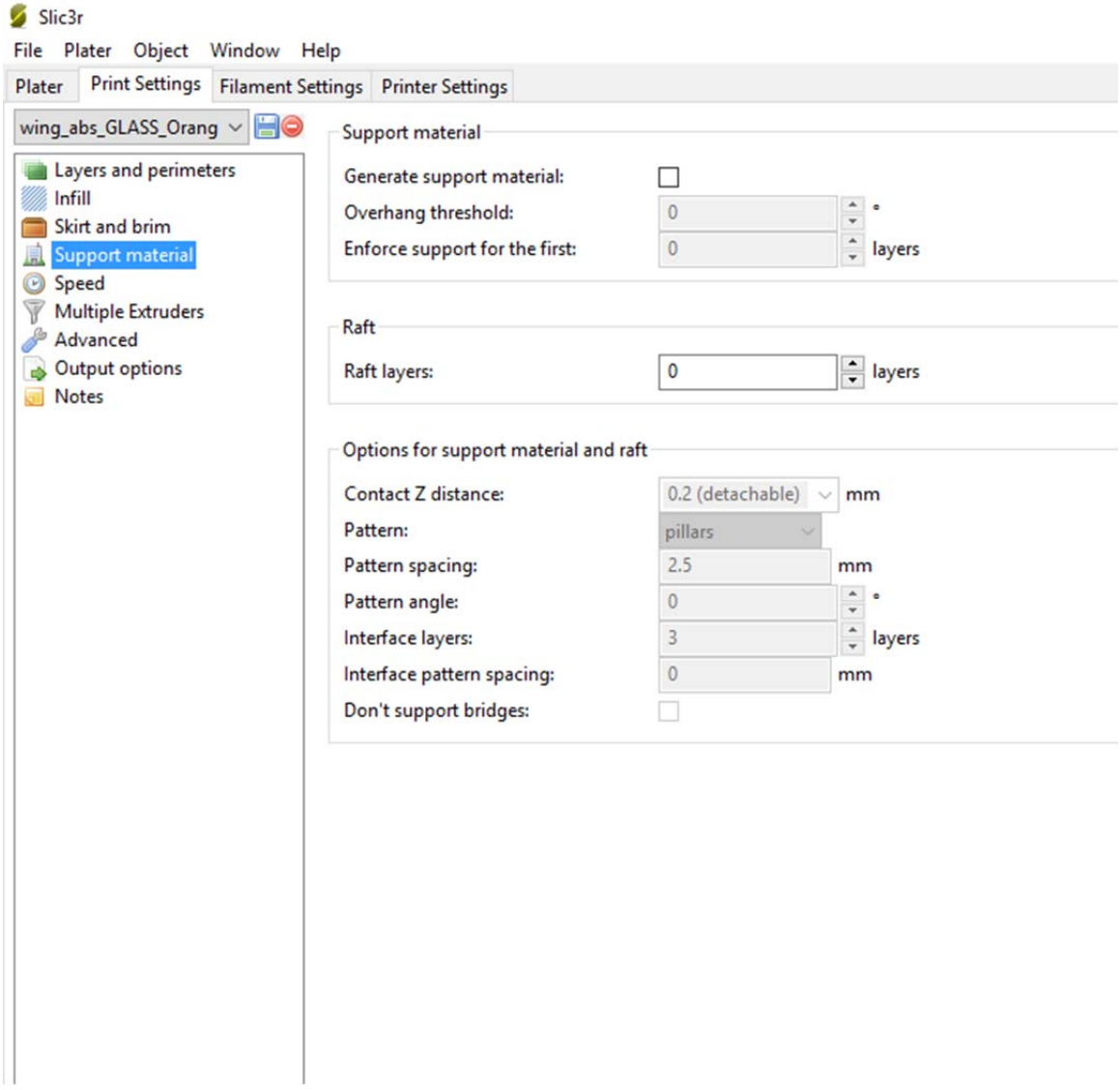
Slic3r
File Plater Object Window Help
Plater Print Settings Filament Settings Printer Settings
wing_abs_GLASS_Orang
Layers and perimeters
Infill
Skirt and brim
Support material
Speed
Multiple Extruders
Advanced
Output options
Notes
Support material
Generate support material:
Overhang threshold: 0 °
Enforce support for the first: 0 layers
Raft
Raft layers: 0 layers
Options for support material and raft
Contact Z distance: 0.2 (detachable) mm
Pattern: pillars
Pattern spacing: 2.5 mm
Pattern angle: 0 °
Interface layers: 3 layers
Interface pattern spacing: 0 mm
Don't support bridges:

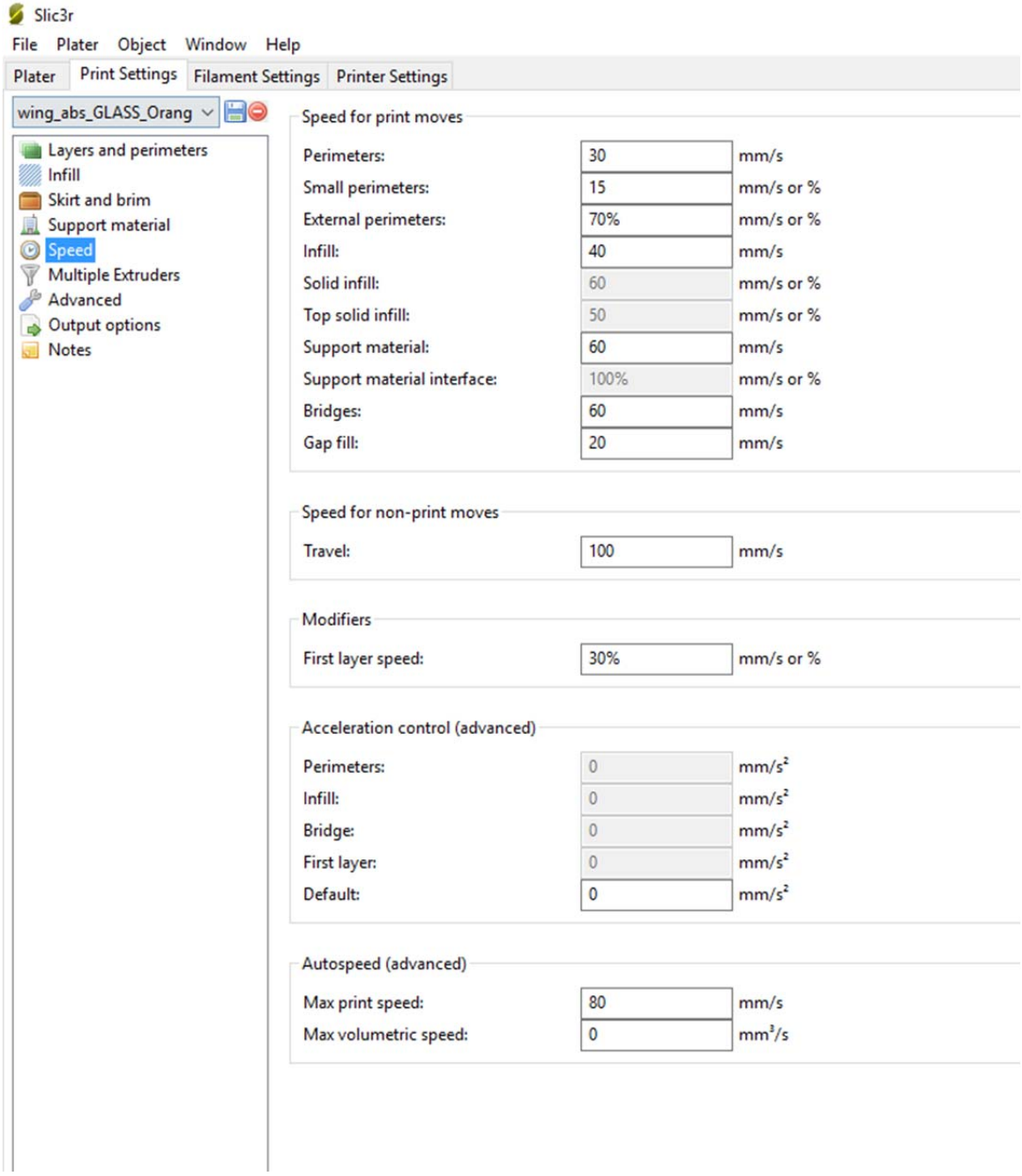
Slic3r
File Plater Object Window Help
Plater
Print Settings
Filament Settings
Printer Settings
wing_abs_GLASS_Orang
Layers and perimeters
Infill
Skirt and brim
Support material
Speed
Multiple Extruders
Advanced
Output options
Notes
Speed for print moves
Perimeters: 30 mm/s
Small perimeters: 15 mm/s or %
External perimeters: 70% mm/s or %
Infill: 40 mm/s
Solid infill: 60 mm/s or %
Top solid infill: 50 mm/s or %
Support material: 60 mm/s
Support material interface: 100% mm/s or %
Bridges: 60 mm/s
Gap fill: 20 mm/s
Speed for non-print moves
Travel: 100 mm/s
Modifiers
First layer speed: 30% mm/s or %
Acceleration control (advanced)
Perimeters: 0 mm/s²
Infill: 0 mm/s²
Bridge: 0 mm/s²
First layer: 0 mm/s²
Default: 0 mm/s²
Autospeed (advanced)
Max print speed: 80 mm/s
Max volumetric speed: 0 mm³/s

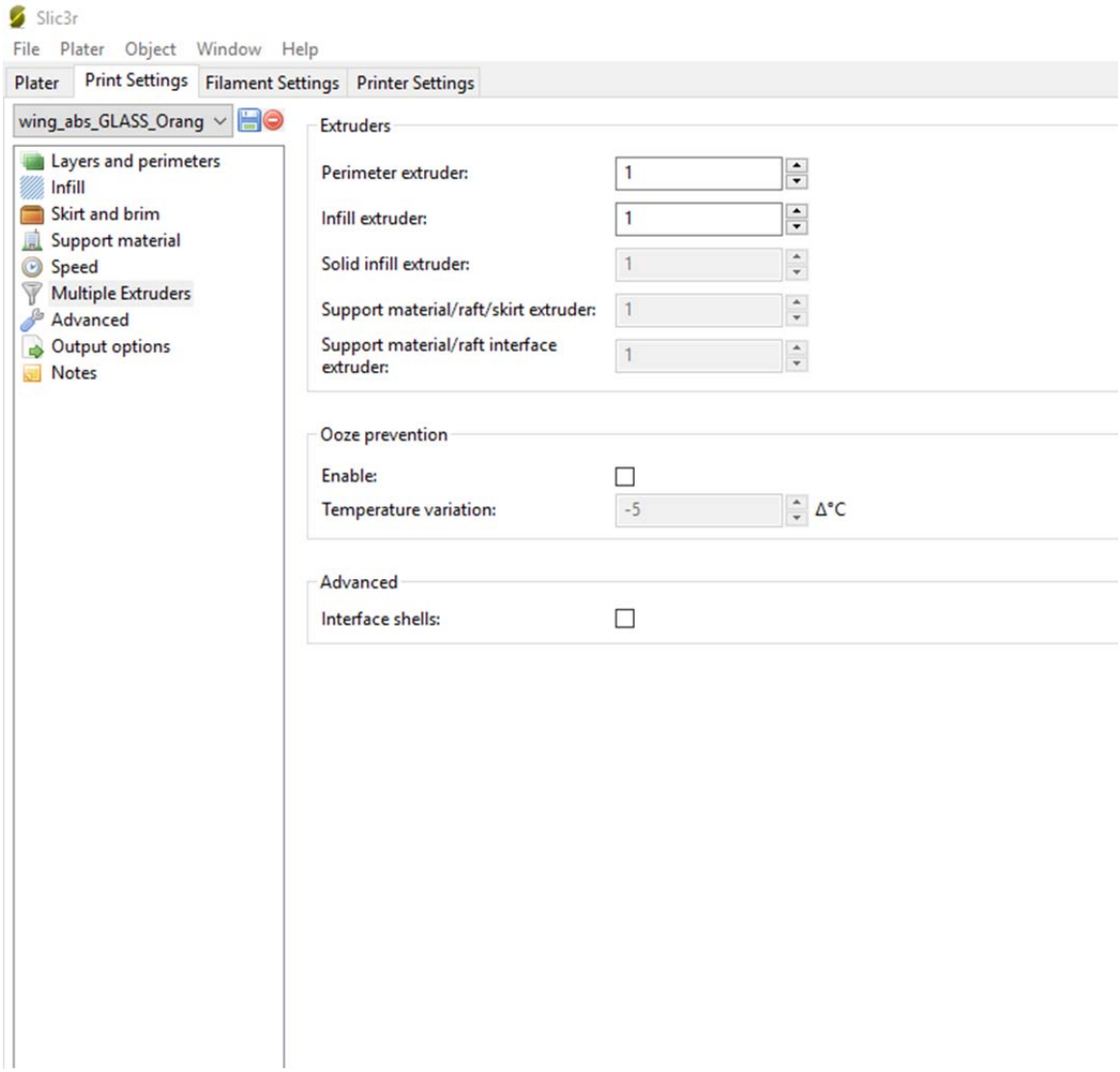
Slic3r
File Plater Object Window Help
Plater
Print Settings
Filament Settings
Printer Settings
wing_abs_GLASS_Orang
Layers and perimeters
Infill
Skirt and brim
Support material
Speed
Multiple Extruders
Advanced
Output options
Notes
Extruders
Perimeter extruder:
1
Infill extruder:
1
Solid infill extruder:
1
Support material/raft/skirt extruder:
1
Support material/raft interface extruder:
1
Ooze prevention
Enable:
Temperature variation:
-5
Δ°C
Advanced
Interface shells:

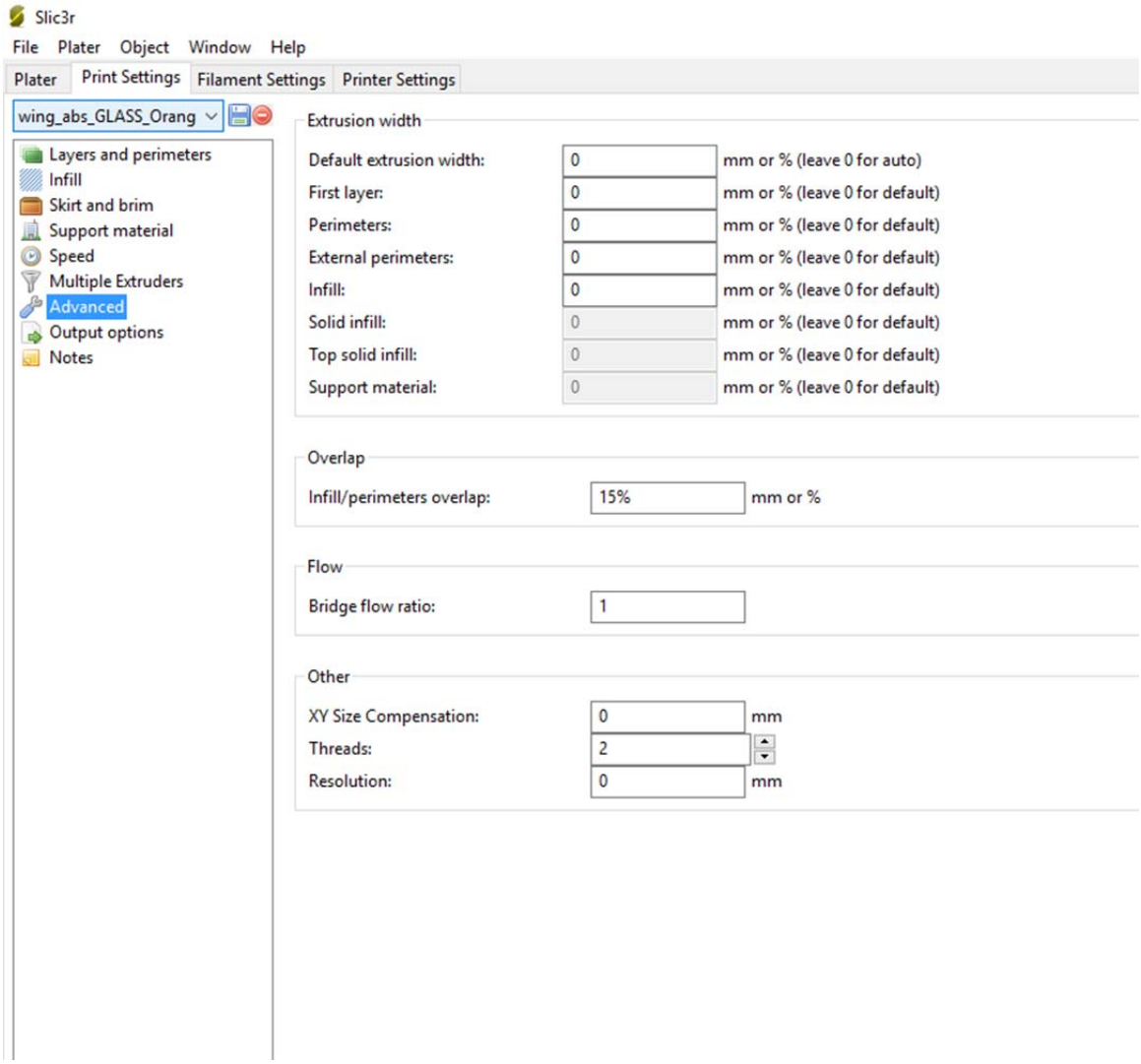
Slic3r
File Plater Object Window Help
Plater Print Settings Filament Settings Printer Settings
wing_abs_GLASS_Orang
Layers and perimeters
Infill
Skirt and brim
Support material
Speed
Multiple Extruders
Advanced
Output options
Notes
Extrusion width
Default extrusion width: 0 mm or % (leave 0 for auto)
First layer: 0 mm or % (leave 0 for default)
Perimeters: 0 mm or % (leave 0 for default)
External perimeters: 0 mm or % (leave 0 for default)
Infill: 0 mm or % (leave 0 for default)
Solid infill: 0 mm or % (leave 0 for default)
Top solid infill: 0 mm or % (leave 0 for default)
Support material: 0 mm or % (leave 0 for default)
Overlap
Infill/perimeters overlap: 15% mm or %
Flow
Bridge flow ratio: 1
Other
XY Size Compensation: 0 mm
Threads: 2
Resolution: 0 mm

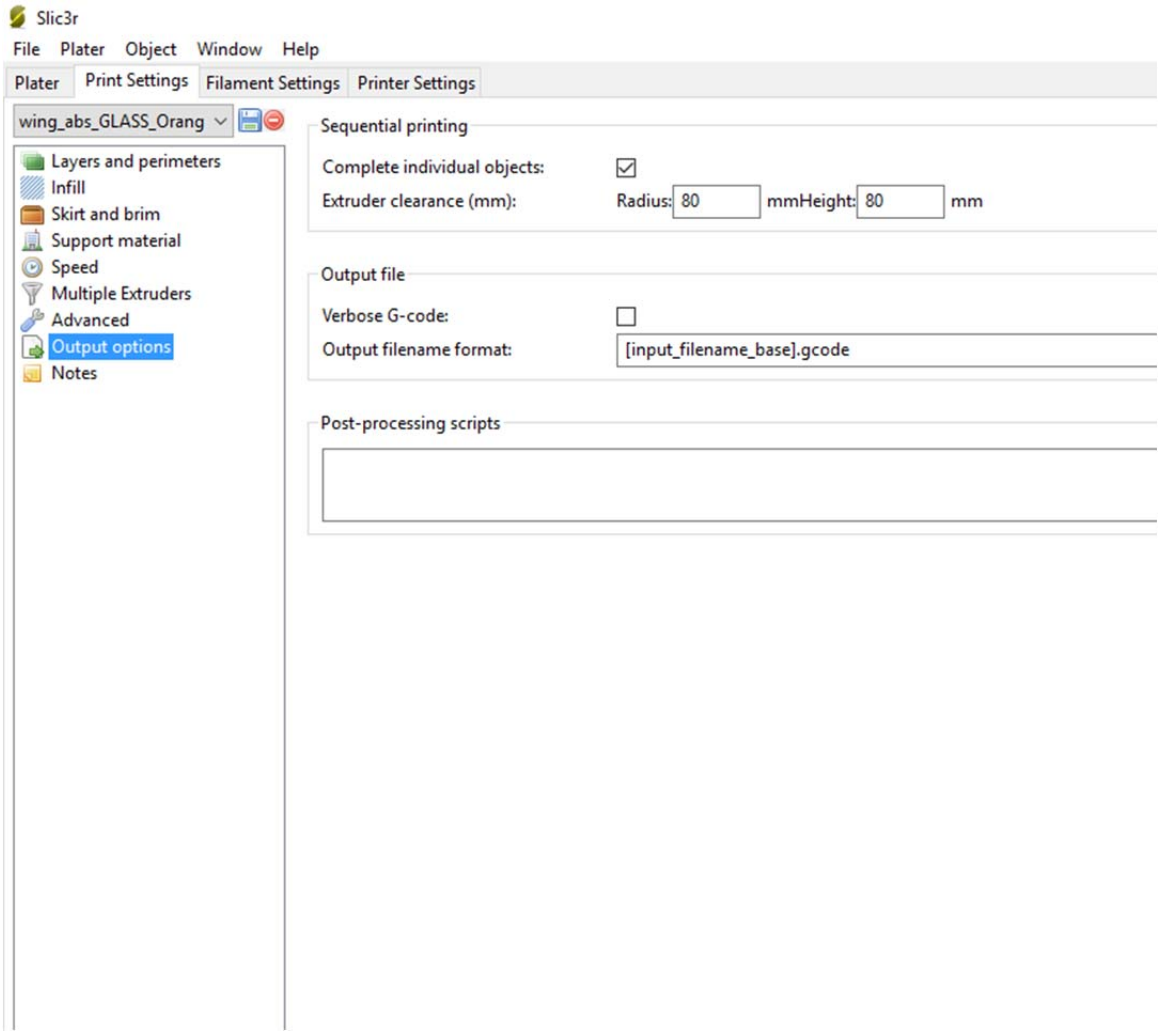
Slic3r
File Plater Object Window Help
Plater
Print Settings
Filament Settings
Printer Settings
wing_abs_GLASS_Orang
Layers and perimeters
Infill
Skirt and brim
Support material
Speed
Multiple Extruders
Advanced
Output options
Notes
Sequential printing
Complete individual objects:
Extruder clearance (mm):
Radius: 80
mmHeight: 80
mm
Output file
Verbose G-code:
Output filename format:
[input_filename_base].gcode
Post-processing scripts

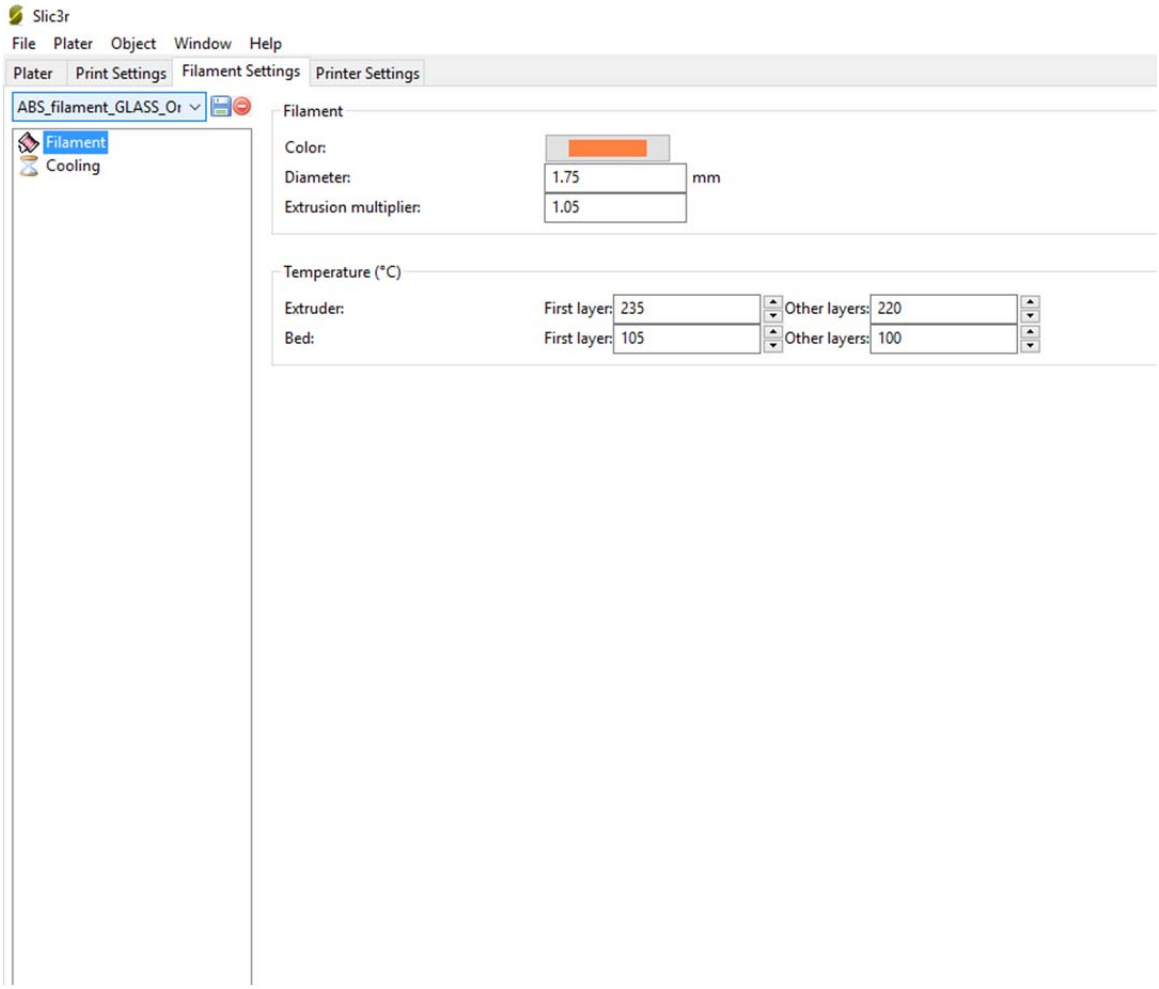
Slic3r
File Plater Object Window Help
Plater Print Settings Filament Settings Printer Settings
ABS_filament_GLASS_Or
Filament
Cooling
Filament
Color:
Diameter: 1.75 mm
Extrusion multiplier: 1.05
Temperature (°C)
Extruder: First layer: 235 Other layers: 220
Bed: First layer: 105 Other layers: 100

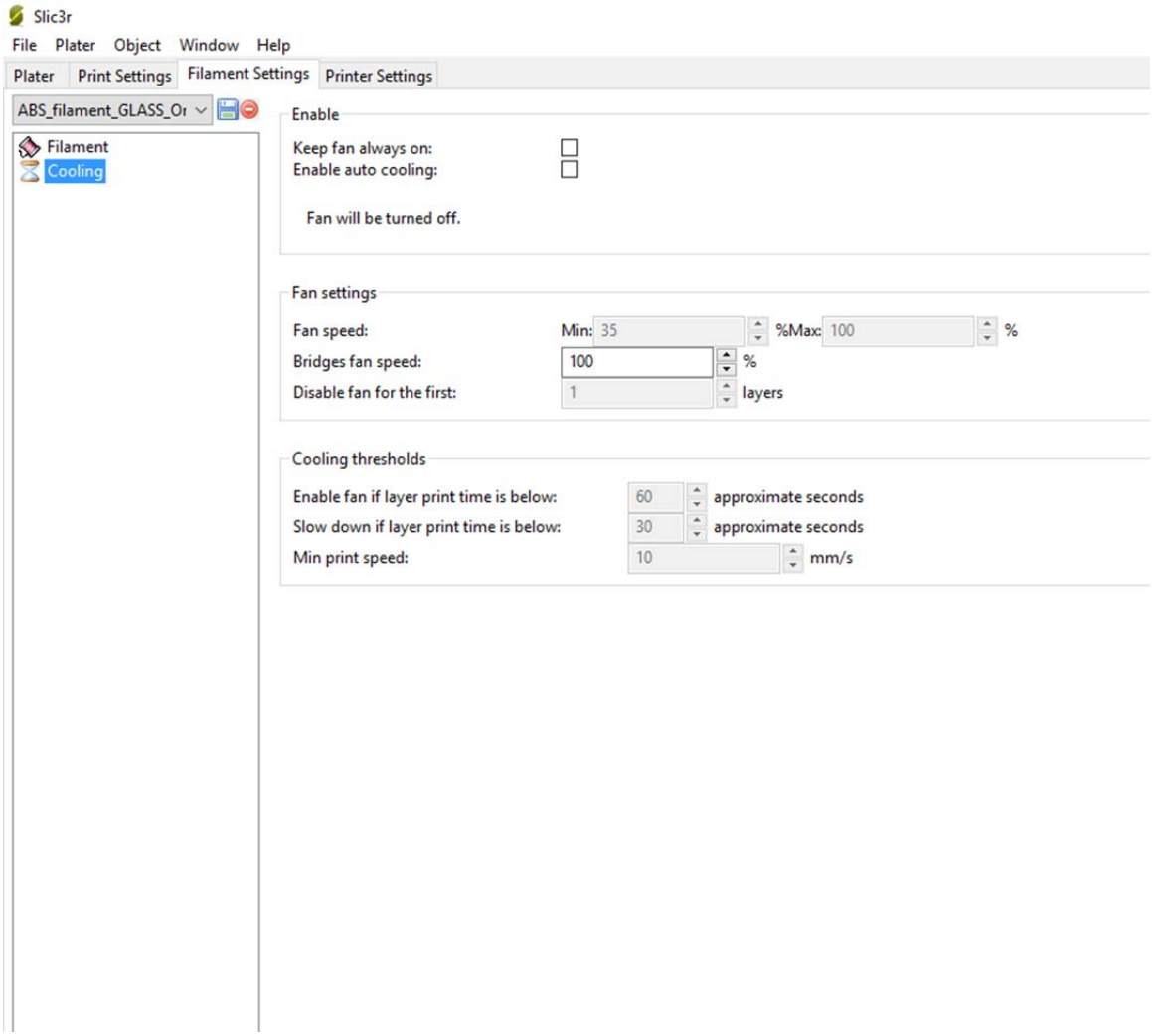
Slic3r
File Plater Object Window Help
Plater Print Settings Filament Settings Printer Settings
ABS_filament_GLASS_Or
Filament
Cooling
Enable
Keep fan always on:
Enable auto cooling:
Fan will be turned off.
Fan settings
Fan speed:
Min: 35
%Max: 100
%
Bridges fan speed:
100
%
Disable fan for the first:
1
layers
Cooling thresholds
Enable fan if layer print time is below:
60
approximate seconds
Slow down if layer print time is below:
30
approximate seconds
Min print speed:
10
mm/s

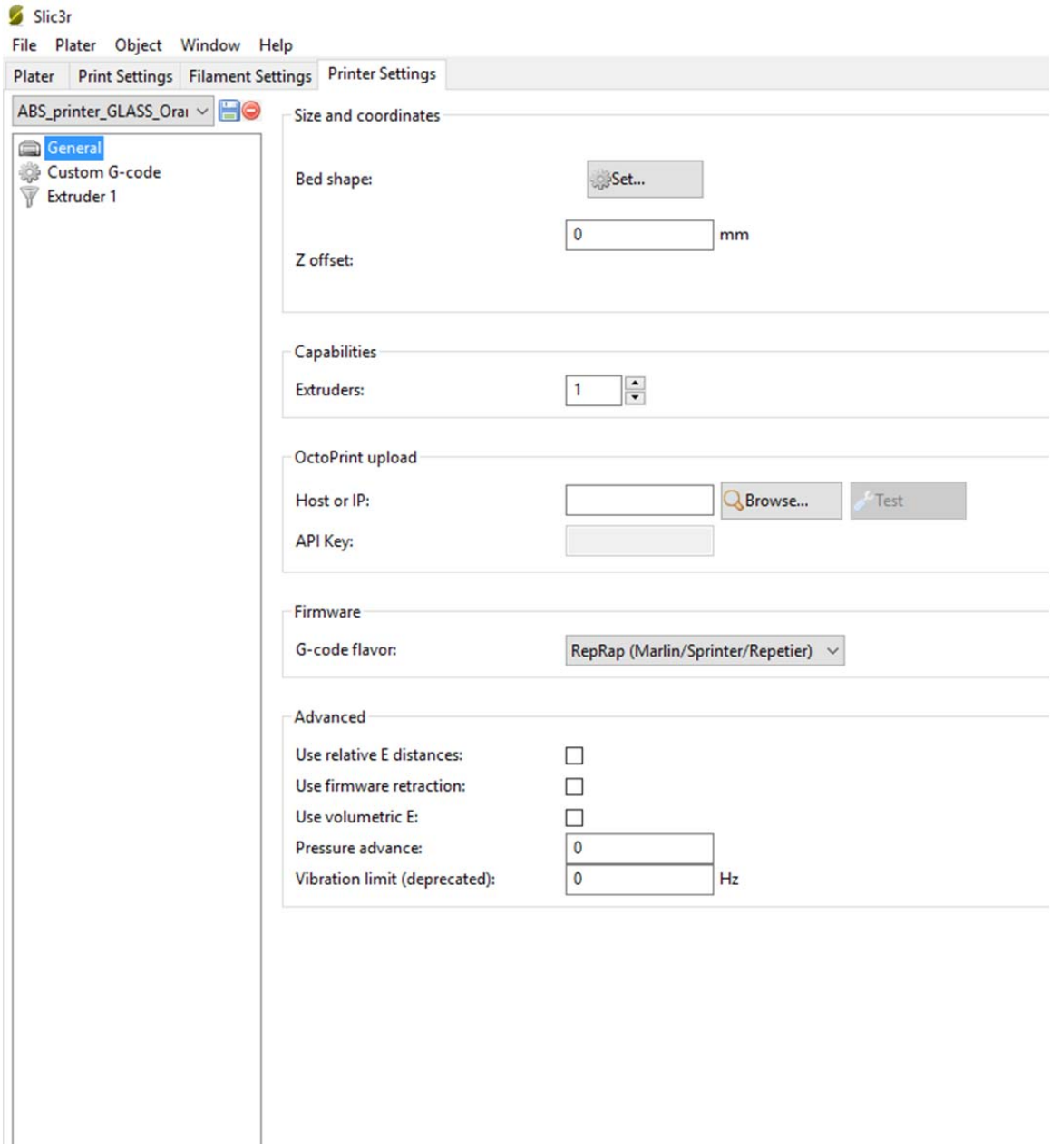
Slic3r
File Plater Object Window Help
Plater Print Settings Filament Settings Printer Settings
ABS_printer_GLASS_Orai
General
Custom G-code
Extruder 1
Size and coordinates
Bed shape:
Set...
Z offset:
0
mm
Capabilities
Extruders:
1
OctoPrint upload
Host or IP:
Browse...
Test
API Key:
Firmware
G-code flavor:
RepRap (Marlin/Sprinter/Repetier)
Advanced
Use relative E distances:
Use firmware retraction:
Use volumetric E:
Pressure advance:
0
Vibration limit (deprecated):
0
Hz

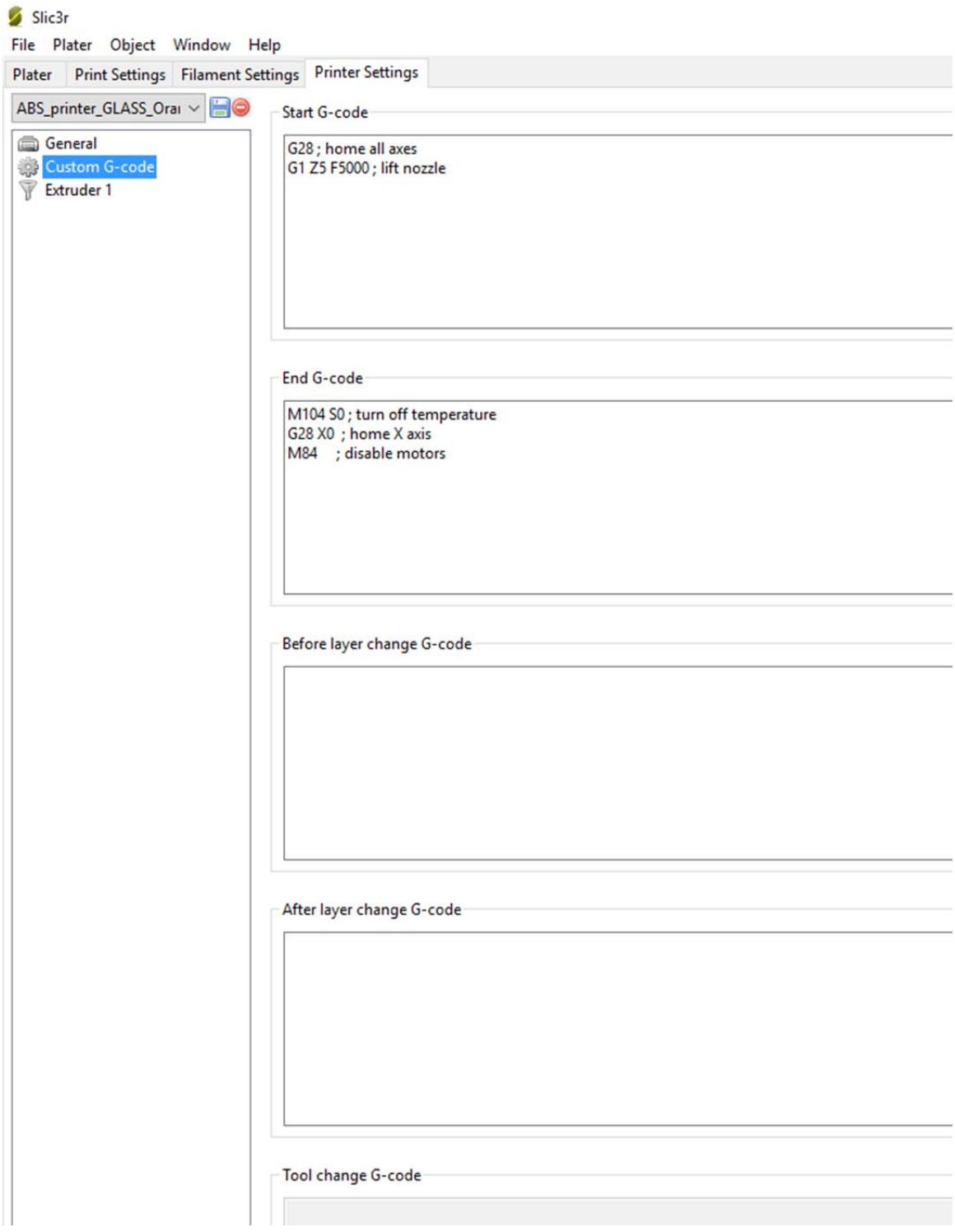
Slic3r
File Plater Object Window Help
Plater Print Settings Filament Settings Printer Settings
ABS_printer_GLASS_Orai
General
Custom G-code
Extruder 1
Start G-code
G28 ; home all axes
G1 Z5 F5000 ; lift nozzle
End G-code
M104 S0 ; turn off temperature
G28 X0 ; home X axis
M84 ; disable motors
Before layer change G-code
After layer change G-code
Tool change G-code

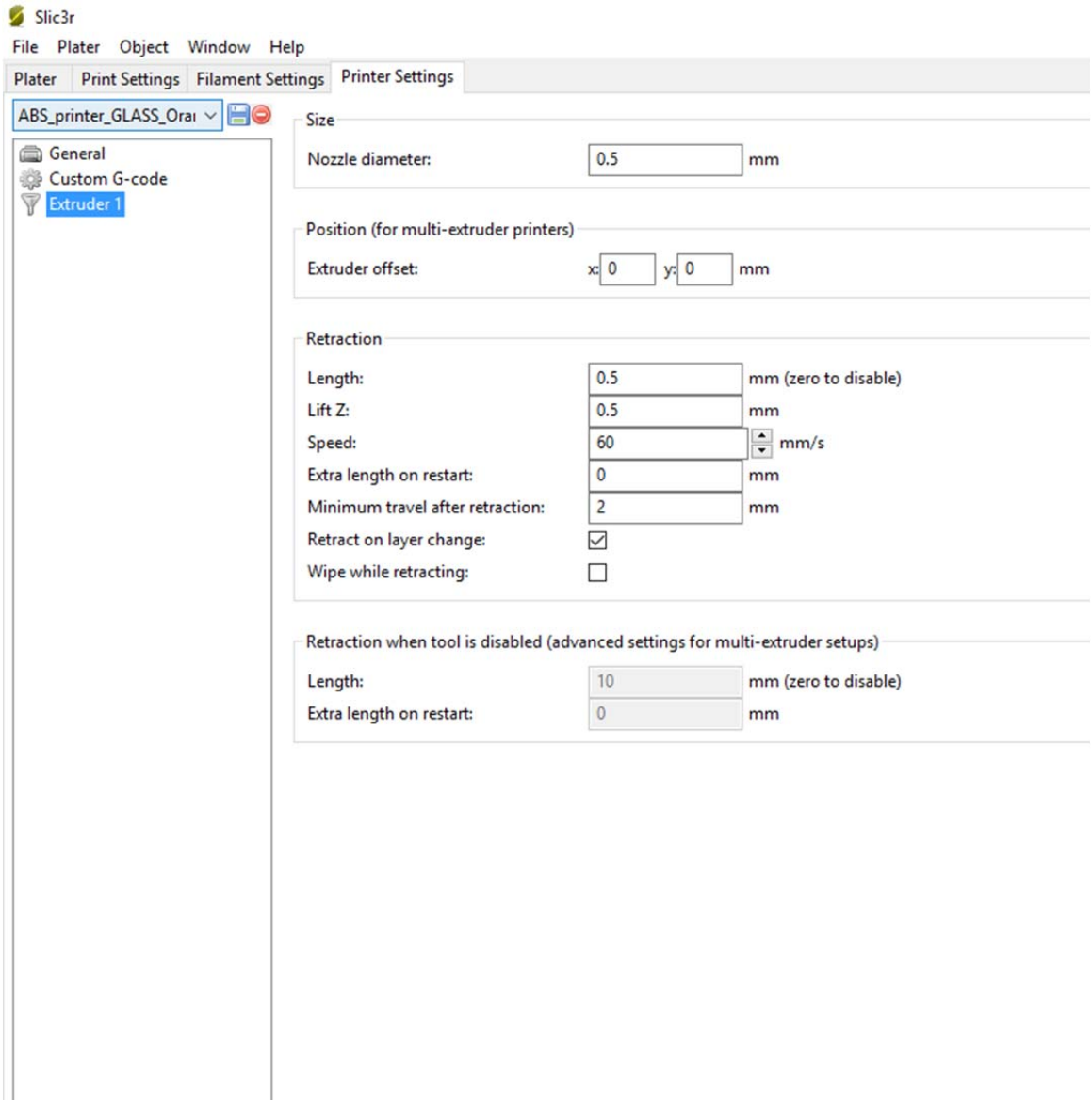
Slic3r
File Plater Object Window Help
Plater Print Settings Filament Settings Printer Settings
ABS_printer_GLASS_Ora
General
Custom G-code
Extruder 1
Size
Nozzle diameter: 0.5 mm
Position (for multi-extruder printers)
Extruder offset: x: 0 y: 0 mm
Retraction
Length: 0.5 mm (zero to disable)
Lift Z: 0.5 mm
Speed: 60 mm/s
Extra length on restart: 0 mm
Minimum travel after retraction: 2 mm
Retract on layer change:
Wipe while retracting:
Retraction when tool is disabled (advanced settings for multi-extruder setups)
Length: 10 mm (zero to disable)
Extra length on restart: 0 mm

THIS PAGE INTENTIONALLY LEFT BLANK

APPENDIX E. NAZA-M FLIGHT CONTROLLER SETTINGS

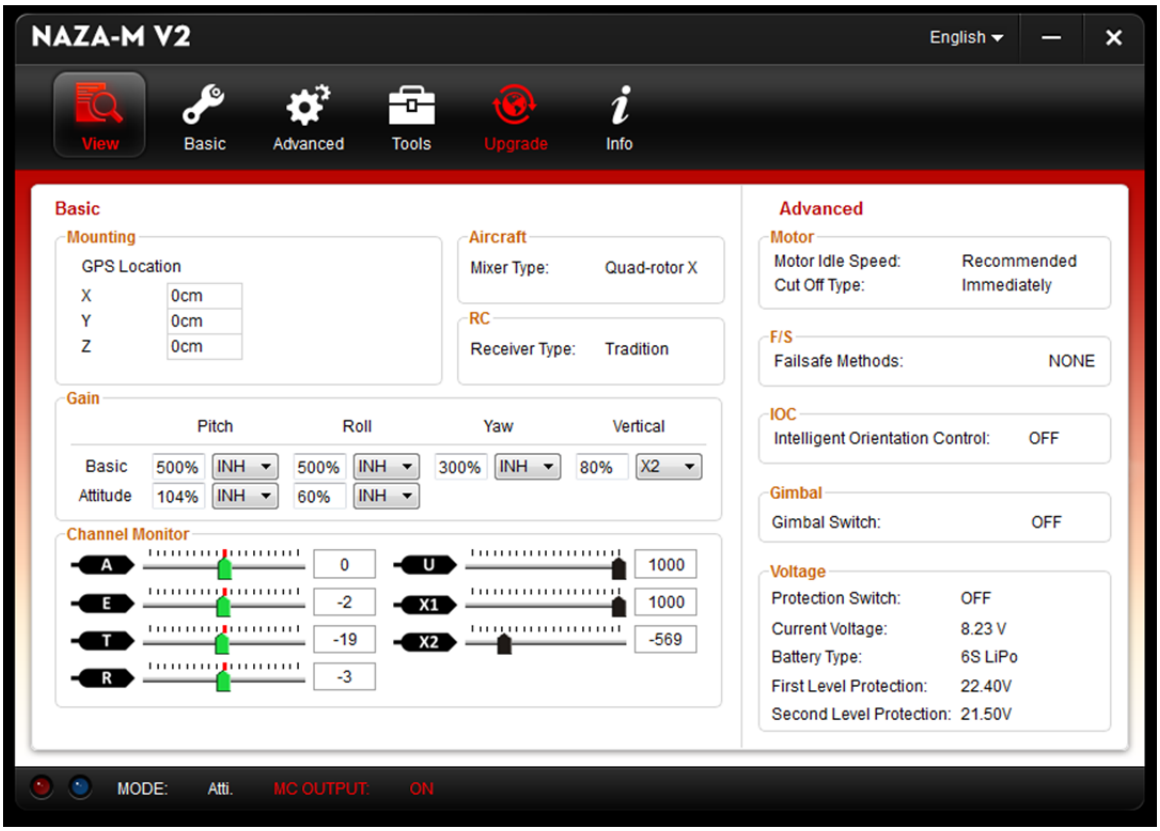

THIS PAGE INTENTIONALLY LEFT BLANK

APPENDIX F. SCORPION MOTOR DATA

	Price ($)	Diameter (mm)	Length (mm)	Kv (RPM/V)	No Load Current @ 10V (A)	Max Cont Current (A)	Max Cont Power (W)	Weight (g)	Max Voltge (V)
HK	500	45	40	400	1.65	150	10000	719	18
HK	1000	70	50	340	6.2	200	10000	1700	13.5
HKIII	350	50	35	500	2.05	120	5400	732	12
HK	350	45	30	450	1.71	110	5400	565	14
HK	375	45	35	500	1.84	100	5180	660	14
HK	375	45	35	450	1.84	100	5180	660	14
HKIII	350	50	35	410	1.53	105	5100	742	12
SII	400	65	30	180	1.26	110	4850	1043	12
HK	350	45	30	540	2.11	115	4800	565	12
HK	350	45	30	500	2.11	115	4800	565	12
HKIII	350	50	35	380	1.44	99	4800	744	14
HK	300	50	35	410	2.12	105	4660	670	12
HKII	300	42	35	520	2.3	100	4550	519	12
HK	300	45	25	520	1.75	100	4450	487	12
HKIII	200	40	35	560	2.24	100	4200	460	12
HKIII	300	50	25	440	1.15	95	4200	566	12
SII	360	55	35	190	1.24	99	4200	906	12
SII	400	65	30	150	1.15	95	4200	1043	12
HKIII	260	50	20	520	1.26	90	4000	498	12
SII	310	55	25	210	1.11	90	4000	708	12
SII	360	55	35	160	1.11	90	4000	906	12
HK	260	50	20	450	1.21	85	3770	445	12
HKIII	260	50	20	450	1.31	85	3770	501	12
HKII	245	42	25	610	2.33	90	3550	393	12
HKII	245	42	25	550	1.77	80	3550	393	12
HKII	245	42	25	500	1.62	80	3550	393	12
HKIII	200	40	35	500	2.02	84	3500	460	12
HKIII	200	40	35	530	2.15	80	3400	460	12
SII	310	55	25	195	0.88	80	3350	708	12
HKIII	200	40	35	450	1.85	75	3300	460	12
S	330	50	30	220	1.03	70	3100	606	12
SII	310	55	25	170	0.78	70	3100	708	12
HKIII	200	40	35	330	1.33	60	2650	460	12
S	350	50	28	220	0.98	70	2590	576	10

THIS PAGE INTENTIONALLY LEFT BLANK

LIST OF REFERENCES

[1] P. Mortier, "Fan or Blowing apparatus," U.S. Patent 507445, 24 October 1893.

[2] M. J. Martin, "Development of a Cross-Flow Fan Rotor for Vertical Take-Off and Landing Aircraft," M.S. thesis, Mechanical and Aerospace Engineering, Naval Postgraduate School, Monterey, CA, 2013.

[3] W. F. Foshag and G. D. Boshler, "USAAVLABS Technical Report 69-13 Review and Preliminary Evaluation of Lifting Horizontal-Axis Rotating-Wing Aeronautical Systems (HARWAS)," U.S. Army Aviation Material Laboratories, Fort Eustis, VA, 1969.

[4] J. D. Kummer, "Simulation of the Cross-Flow Fan and Application to a Propulsive Airfoil Concept," Syracuse University, Syracuse, 2006.

[5] E. D. Smitley, "Development of a Cross-Flow Fan Powered Quad-Rotor Unmanned Aerial Vehicle," M.S. thesis, Mechanical and Aerospace Engineering, Naval Postgraduate School, Monterey, CA, 2015.

[6] Amazon, "Amazon Prime Air," 29 November 2015. [Online]. Available: http://www.amazon.com/b?node=8037720011. [Accessed 12 March 2016].

[7] "V-22 Osprey," Boeing, 2016. [Online]. Available: http://www.boeing.com/defense/v-22-osprey/#/gallery. [Accessed 25 May 2016].

[8] O. G. Tietjens, *Applied Hydro- and Aeromechanics*, New York: McGraw-Hill Book Company, Inc., 1934.

[9] E. B. Wolff, "Preliminary Investigation of the Effect of a Rotating Cylinder in a Wing," National Advisory Committee for Aeronautics, Amsterdam, Netherlands Mar. 1925.

[10] M. F. Platzer, private communication, Feb. 2016.

[11] D. L. Kohlman, *Introduction to V/STOL Airplanes*, Ames: The Iowa State University Press, 1981.

[12] T. Q. Dang and P. R. Bushnell, "Aerodynamics of cross-flow fans and their appliction to the aircraft propulsion and flow control," *Progress in Aerospace Sciences,* vol. 45, pp. 1-29, 2009.

[13] R. K. Dygert and T. Q. Dang, "Experimental Investigation of an Embedded Crossflow Fan for Airfoil Propulsion/Circulation Control," *Journal of Propulsion and Power,* vol. 25, no. 1, pp. 196, Feb. 2009.

[14] C. Gologan, S. Mores, H.-J. Steiner and A. Seitz, "Potential of the Cross-Flow Fan for Powered-Lift Regional Aircraft Applications," in *AIAA Aviation Technology, Integration, and Operations Conference*, Hilton Head, SC, 2009.

[15] A. M. Jones, "Integration of Twenty-bladed Cross-flow Fan into Vertical Take-off and Landing Aircraft," M.S. thesis, Mechanical and Aerospace Engineering, Naval Postgraduate School, Monterey, CA 2013.

[16] UIUC Airfoil Coordinates Database. Gottinggen 570 Airfoil Profile. [Online]. Available: http://m-selig.ae.illinois.edu/ads/afplots/goe570.gif. Accessed Apr., 20, 2016.

[17] F. M. White, *Fluid Mechanics*, 7th ed, New York: McGraw-Hill, 2011, pp. 363-364.

[18] Fibre Glast Developments Corporation, "Product Data Sheet," 2010. [Online]. Available: http://cdn.fibreglast.com/downloads/00941-A.pdf. [Accessed 1 January 2016].

[19] "Simplify3D Print Quality Troubleshooting," 2016. [Online]. Available: https://www.simplify3d.com/support/print-quality-troubleshooting/. [Accessed 17 March 2016].

[20] T. Landry, "MatterHackers ABS Bed Adhesion Tips & Tricks," 2 July 2014. [Online]. Available: https://www.matterhackers.com/articles/printing-tips-&-tricks:-abs-bed-adhesion. [Accessed 30 January 2016].

INITIAL DISTRIBUTION LIST

1. Defense Technical Information Center
   Ft. Belvoir, Virginia

2. Dudley Knox Library
   Naval Postgraduate School
   Monterey, California